JGR Oceans

RESEARCH ARTICLE
10.1029/2023JC020500

Hurricane-Driven Transport of Bermuda Reef Carbonate Platform Sediments to the Deep Ocean

R. Pedrosa-Pamies[1], M. H. Conte[1,2], J. C. Weber[1], and A. J. Andersson[3]

[1]The Ecosystems Center, Marine Biological Laboratory, Woods Hole, MA, USA, [2]Bermuda Institute of Ocean Sciences, St. George's, Bermuda, [3]Scripps Institution of Oceanography, University of California San Diego, La Jolla, CA, USA

Key Points:

- First study to document real-time in situ transport of platform sediments to depth by hurricane-induced internal wave/slope interactions
- Transport of aragonite and high-Mg calcites to depth bolster deep ocean alkalinity upon dissolution, aiding neutralization of anthropogenic CO_2
- Hurricanes also transport phosphorus, lithogenic and authigenic minerals, and pollutants stored in deep slope sediments to the deep ocean

Supporting Information:

Supporting Information may be found in the online version of this article.

Correspondence to:

R. Pedrosa-Pamies, rpedrosa@mbl.edu; rutpedpam@gmail.com

Citation:

Pedrosa-Pamies, R., Conte, M. H., Weber, J. C., & Andersson, A. J. (2025). Hurricane-driven transport of Bermuda reef carbonate platform sediments to the deep ocean. *Journal of Geophysical Research: Oceans*, *130*, e2023JC020500. https://doi.org/10.1029/2023JC020500

Received 19 SEP 2023
Accepted 13 FEB 2025

Author Contributions:

Conceptualization: R. Pedrosa-Pamies, M. H. Conte
Data curation: R. Pedrosa-Pamies, M. H. Conte, J. C. Weber
Formal analysis: R. Pedrosa-Pamies, M. H. Conte, J. C. Weber, A. J. Andersson
Funding acquisition: M. H. Conte
Investigation: R. Pedrosa-Pamies, M. H. Conte, J. C. Weber
Methodology: R. Pedrosa-Pamies, M. H. Conte, J. C. Weber
Project administration: R. Pedrosa-Pamies, M. H. Conte
Software: R. Pedrosa-Pamies
Supervision: R. Pedrosa-Pamies
Visualization: R. Pedrosa-Pamies
Writing – original draft: R. Pedrosa-Pamies
Writing – review & editing: R. Pedrosa-Pamies, M. H. Conte, J. C. Weber, A. J. Andersson

Abstract Tropical cyclones erode and remobilize coastal sediments but their impact on the deep ocean remains unclear. Hurricane-driven transport of carbonates and associated materials from reef carbonate platforms to the deep ocean has important implications for carbon storage, deep ecosystems and ocean chemistry as carbonate platform reef-sourced aragonite and high-Mg calcite (HMC) may dissolve and contribute to deep water total alkalinity. Here we describe two hurricane-driven resuspension events where deep sediment plumes from the Bermuda Pedestal (NW Atlantic) were advected to deep waters surrounding the Oceanic Flux Program (OFP) mooring site, ~75 km southeast of Bermuda. Hurricanes Fabian (Cat. 3, 2003) and Igor (Cat. 1, 2010) generated large near-inertial waves propagating to >750 m depths, leading to widespread sediment resuspension from the Pedestal. Following Fabian, carbonate fluxes at the OFP site increased 15-fold, 32-fold, and 6-fold at 500, 1,500 and 3,200 m, respectively, with the 1,500 m flux equivalent to the total annual carbonate flux. OFP traps similarly captured a large detrital carbonate plume following Igor; here, the plume was shallower and persisted longer. Microscopy, geochemistry, and mineralogy confirmed that both plumes consisted of fine-grained shallow-water detrital carbonates alongside other materials accumulated on the Pedestal including phosphorus, lithogenic, authigenic, and pollutant elements. Clay-sized particles (<4 μm) in both plumes exhibited high contents of lithogenic and authigenic elements, and Zn, Cd, and V, facilitating their transport over long distances. Grain-size, elemental, and lipid composition indicated that plumes intercepted at different depths originated from different source areas on the Pedestal.

Plain Language Summary This study demonstrates, for the first time, hurricane-induced transport of deep sediments from reef carbonate platforms to the deep ocean in near-real time. This phenomenon has important implications for the marine carbon cycle because carbonate platform-derived carbonates may dissolve in the deep ocean and contribute to its buffering and carbon storage capacities. Our paper focuses on two hurricanes, Hurricane Fabian in 2003 and Hurricane Igor in 2010, that resuspended large amounts of sediment from the Bermuda Pedestal, generating large plumes of detrital carbonate sediments that were transported offshore to the deep waters surrounding the Oceanic Flux Program (OFP) mooring site 75 km southeast of Bermuda. Fabian delivered a year's worth of the carbonate flux to the deep ocean in only 2 weeks. Hurricane-driven resuspension and offshore transport of carbonate platform sediments is also important for ocean chemistry and deep ocean ecosystems as this process also transports phosphorus, lithogenic and authigenic minerals, and pollutants, such as lead, that accumulate in reef platform sediments to the deep ocean.

1. Introduction

Shallow-water reefs, globally distributed throughout the tropics and subtropics, build extensive flat-topped reef rimmed carbonate platforms (Pomar & Hallock, 2008), such as those found in the Caribbean, Red Sea, Indo-Pacific islands, and Great Barrier Reef (Laugié et al., 2019; Michel et al., 2019). Reef carbonate platforms (active reefs as well as adjacent lagoons) play an essential role in sedimentary processes shaping geomorphological features of the shelf, slope, and basin environments (Markello et al., 2008; Thran et al., 2020; Tucker et al., 1990).

Carbonate platforms are important components in the marine carbon cycle. Globally, coral reefs are estimated to account for ~50% of shallow water carbonate production and >25% of the carbonate buried in marine sediments (Jones et al., 2015; Milliman, 1993). Platform carbonates largely consist of metastable detrital aragonite and magnesian calcite synthesized by corals, coralline algae, and other carbonate-producing reef organisms (e.g., Chave, 1954). Thus, offshore transport of carbonate platform-derived sediments to deep waters also affects

seawater chemistry and carbon cycling as detrital aragonitic and magnesian calcite may dissolve in the water column or at the seafloor due to metabolic or environmental dissolution (Andersson, 2014; Milliman, 1993; Sulpis et al., 2021).

Tropical cyclones frequently pass through low-latitude areas having extensive carbonate platforms, providing opportunities for large-scale sediment resuspension and advective redistribution (e.g., Bianucci et al., 2018; Patrick et al., 2022). Multiple factors, including wave intensity, winds, storm tracks, topography, sediment composition, and water depth influence shallow sediment resuspension on carbonate platforms (Fabricius et al., 2008; Harmelin-Vivien, 1994; Jamison-Todd et al., 2020). The shear stress produced by hurricane-generated upper ocean currents and waves can resuspend large volumes of sediments from as deep as ∼100 m water depth (Teague et al., 2007).

Additionally, tropical cyclones also generate strong deep internal waves, which may break along deep slope boundaries and lead to extensive sediment resuspension. Wind-generated inertial motions within the mixed layer radiate near-inertial waves into the ocean's interior (Alford et al., 2016; Kawaguchi et al., 2016), with downward energy propagation influenced by water column structure, circulation, and topography (Cheriton et al., 2021; Spencer et al., 2016; Zedler et al., 2002). Sediment resuspension events related to deep internal waves impinging on the seabed have resulted in turbidity currents and sediment plume formation (Larcombe & Carter, 2004; Liu et al., 2012; Miramontes et al., 2020; van Haren & GostIaux, 2012).

Sediment transport from carbonate platforms to offshore waters is rarely documented by in situ data. Remote sensing can evaluate shallow water sediment resuspension and transport triggered by hurricanes (e.g., Acker et al., 2004, 2010), but remote sensing images are restricted to at most 100 m depth. Rather, most evidence of advection of shallow-water platform carbonates to the deep ocean has been obtained indirectly from topographic/geomorphological studies, and sediment coring of nearshore regions and wash-over fans (e.g., Jamison-Todd et al., 2020; Mattheus & Yovichin, 2018; Spiske et al., 2022), for example, geologic studies of bathymetric data and sediment facies distributions in the Caribbean Islands (Browning et al., 2019; Jamison-Todd et al., 2020) and the Great Barrier Reef in Australia (Larcombe & Carter, 2004).

Morphosedimentary studies have observed the accumulation of fine-grained shallow water carbonates in slope and deep water sediments adjacent to carbonate platforms, evidencing mobilization and transport of carbonate off the platform into surrounding basins. For example, reworked shallow-water carbonate debris is found on the deep margins of the Great Barrier Reef and Less Antilles (Dunbar & Dickens, 2003; Seibert et al., 2020; Thran et al., 2020), the Bahama Bank (Boardman & Neumann, 1984; Heath & Mullins, 1984; A. C. Neumann & Land, 1975), and the Bermuda Platform (Berner et al., 1976; Ericson et al., 1952; James et al., 2023; Mackenzie et al., 1965). Farther offshore Bermuda, Ericson et al. (1952, 1961) additionally documented a thick turbidite sequence of well-sorted detrital carbonate in the abyssal plain southeast of Bermuda, highlighting the role of turbidity currents in sediment transport. We have sampled the same turbidite feature, which consists of a thick carbonate layer approximately 8–12 cm below the seafloor with extensive mixing of turbidite and pelagic sediments at the flow margins (OFP unpublished observations).

Bermuda is the northernmost subtropical coral reef and carbonate platform in the world and is frequently impacted by hurricanes. Since 1960, 46 hurricanes passing through the North Atlantic have passed within 300 km of Bermuda. Approximately 60% of the 46 hurricanes passing near Bermuda since 1960 approached from the south to southwest. Consequently, hurricane-generated swells and waves generally have the greatest impact along the southern and southeastern Pedestal (Smith Warner International, 2004). Previous studies have described how hurricane events impact upper ocean physics and biology (Acker et al., 2010; Black & Dickey, 2008; Dickey, Frye, et al., 1998; Malone et al., 1993; Zedler et al., 2002) and the particle flux (Pedrosa-Pàmies et al., 2018, 2019) in the open ocean.

Here we report the first real-time in situ observations of resuspension, advection and settlement of platform-derived carbonates to offshore deep ocean waters during Hurricanes Fabian 2003 (Cat. 3, Sep. 2003) and Igor 2010 (Cat. 1, Sep. 2010). Both hurricanes induced massive sediment resuspension on the deep slope of the Bermuda Pedestal and transported these sediment plumes offshore to the abyssal plain surrounding the Oceanic Flux Program (OFP) sediment trap time-series mooring site, ∼75 km southeast of Bermuda. Using a suite of microscopic and chemical tracers (major and trace elements, lipids, carbonate isotopic composition, and

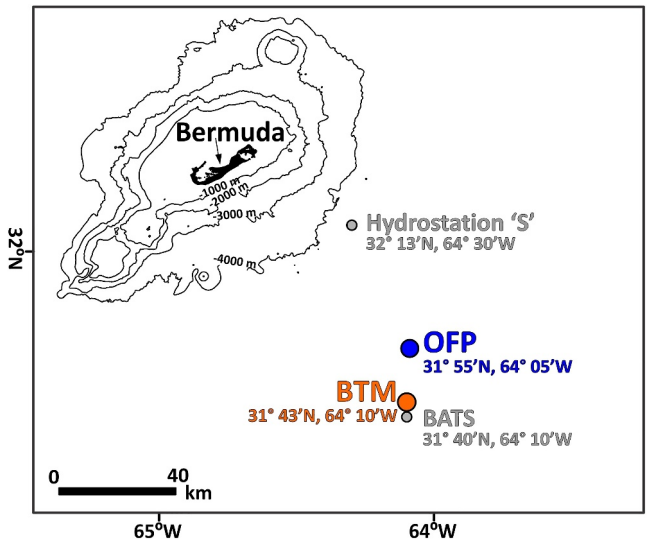

Figure 1. Map of Bermuda bathymetry and the locations of the Oceanic Flux Program (OFP) mooring, the Bermuda Testbed Mooring (BTM), Hydrostation S, and the Bermuda Atlantic Time-series Study (BATS).

mineralogy), we document the plumes' composition and provide evidence that the Fabian and Igor plumes intercepted at different depths by the OFP sediment traps were sourced from different areas on the Pedestal.

2. Study Area

Bermuda is situated in the North Atlantic subtropical gyre about 1,000 km east of Cape Hatteras. The islands lie on an extinct Eocene/Oligocene shield volcano, the Bermuda Pedestal, that measures approximately 130 km by 80 km at its base depth of 4,200 m (Figure 1 and Figure S1 in Supporting Information S1). Capping the Bermuda Pedestal is a shallow (~50 m depth) reef carbonate platform (the Bermuda Platform) of approximately 650 km^2 area (Coates et al., 2013; Courtney et al., 2016; Iliffe et al., 2011; Lavoie & Matthews, 1983; Stanley & Swift, 1968) that is covered with 26–90 m thick veneer of Quaternary carbonate sediment and limestone (Land et al., 1967). The sediment was and is being produced today by corals, calcifying marine algae and a myriad of calcareous invertebrates that thrive in the lagoons, seagrass meadows, and reefs around the islands. The broad upper terrace of the Platform (20–22 m depth) transitions to a distinctively steeper slope starting at ≈55–65 m, which descends almost vertically to ~100 m depth (Coates et al., 2013; Iliffe et al., 2011) (Figure S1 in Supporting Information S1). Seafloor samples collected along the southern margin of the Bermuda reef platform slope between 40 and 468 m depth indicate the presence of limestones: coralline algal boundstones variably constructed with ahermatypic corals, bryozoans, and the hydrozoan *Millepora sp*, and other benthic components such as benthic foraminifera, serpulid worms, and gastropods. Increased abundance of burrowed carbonate sand and silt is observed at the distal slope (230–468 m) (James et al., 2023 and references therein). The Bermuda Pedestal geology has been summarized by Lavoie and Matthews (1983). The Pedestal has significant topographic features such as ridges and canyons (Stanley & Swift, 1968). Its slope is most extreme on its southeastern flank, deepening from 185 to 4,200 m depth over a distance of 37 km (Vacher & Rowe, 2004). At depths below 1,000 m, the Pedestal sediments are a combination of detrital shallow-water reef-derived carbonates remobilized from the Platform sediments (e.g., red and green algae, sponge spicules, bryozoan and coral particles), with lesser amounts of pelagic carbonates (e.g., ostracods, coccoliths, and planktonic forams) (Lavoie & Matthews, 1983). Variability in grain size and carbonate content indicates discontinuous resuspension and deposition of the swallow-water carbonates on the deep Pedestal slope (Ericson et al., 1952; Lavoie & Matthews, 1983). Additionally, the percentage of clay-sized minerals from the erosion of red soils in Bermuda limestone increases on the lower slopes of the Bermuda Pedestal (ibid).

The mineralogy and geochemistry of the Bermuda Platform and Pedestal sediments reflects the shallow-water reef-sources of the carbonate limestones with lesser amounts eolian-derived lithogenic minerals. Calcite and low-Mg-calcite on the Bermuda Platform mostly originate from erosion of limestone and eolianite (Andersson et al., 2007) and biogenic carbonate debris from corals, coralline algae, benthic foraminifera, bryozoans and echinoderms, which is strongly dominated by aragonite and high Mg-calcites (e.g., Chave, 1962; Neumann, 1965). Relative abundances of aragonite, calcite (and low Mg-calcite), and high Mg-calcite ranges from 65%:26%:9% inside Harrington Sound (Andersson et al., 2007; Neumann, 1965), to 68%:11%:22% across the northern reef lagoon (Chave, 1962), to 51%:16%:33% in sediments near active reefs (Figure S1 in Supporting Information S1). The relative contribution of eroded limestone decreases toward the edge of the Platform while contributions from high Mg-calcite calcifiers such as benthic foraminifera and coralline algae increases (e.g., Courtney et al., 2016), resulting in increased relative concentrations of high Mg-calcites to ~40% at the Platform edge (Chave, 1962; Andersson, unpublished data).

The detrital carbonate composition deeper on the Bermuda Pedestal slope reflects its shallow-water origin and diagenetic alterations. Between 1,000 m and 2,000 m depths, the relative percentages of carbonate minerals average 28%–37% aragonite, 13%–29% calcite and 34%–50% high Mg-calcite (Berner et al., 1976; Lavoie & Matthews, 1983). Seawater saturation with respect to carbonate mineral phases decreases as a function depth and becomes undersaturated below the depth where the mineral specific solubility product equals the in situ ion concentration product (i.e., $\Omega = 1$; saturation horizon) favoring net dissolution of aragonite and high Mg-calcite

(aragonite saturation horizon depth ~2,400 m). This leads to an increasing relative abundance of calcite on the deeper slopes of the Pedestal. For example, below 3,000 m depth 84% of the carbonate composition is comprised of calcite with aragonite and high Mg-calcite making up only 5% and 11%, respectively (Berner et al., 1976).The Bermuda Time-Series Site (Figure 1) southeast of Bermuda hosts several ongoing time-series: the Hydrostation S (since 1954) time-series of hydrographic parameters (Michaels & Knap, 1996; Phillips & Joyce, 2007; Steinberg et al., 2001), the Oceanic Flux Program (OFP, since 1978) time-series of deep ocean particle fluxes (Conte et al., 2001, 2025; Conte & Weber, 2014; Deuser, 1986), and the Bermuda Atlantic Time-series Study (BATS, since 1988) of upper ocean biogeochemistry (Lomas et al., 2013; Michaels & Knap, 1996; Steinberg et al., 2001). The OFP time-series has continuously measured the deep particle flux at 3,200 m depth since 1978, and at 500 and 1,500 m depth since 1984, with a temporal coverage of >90%. Between 1995 and 2007, the Bermuda Testbed Mooring (BTM) time-series of ocean physical and optical properties in the upper 750 m was located just south of the OFP site (Dickey et al., 2001).

3. Methods

3.1. Remote Sensing Data

Hurricane information was obtained from the National Oceanic and Atmospheric Administration (NOAA) National Hurricane Center (NHC)'s post analysis data product of hurricane position and intensity. Hurricane translational speed was calculated using centered time differencing of changes in longitude and latitude at 6-hr interval.

Satellite images were obtained from NASA's Modis Aqua and Terra satellite products distributed by NASA's Goddard Earth Sciences Data, Information Services Center (Ocean Biology Processing Group). Sea surface temperature (SST) was obtained from the Moderate Resolution Imaging Spectrometer on the Aqua platform, using 4-km resolution Level 3 binned data. Sea surface height (SSH) data were obtained from the daily outputs of the operational Mercator global analysis (spatial resolution of $0.083° \times 0.083°$).

3.2. Hydrographic Data

Bermuda Testbed Mooring (BTM) deployment #18 continuously collected temperature profiles during Hurricane Fabian 2003 using Seabird MicroCATs (SeaBird Instruments, Bellevue WA) located at 2, 8, 19, 35, 47, 57, 72, 101, 151, 201, 501, and 751 m depths. Details of the BTM measurements are provided in Black and Dickey (2008). Horizontal current measurements were obtained with an upward-looking RDI 150 KHz Acoustic Doppler Current Profiler located at 201 m depth, and with data averaged every 15 min and binned within 3-m vertical intervals with the deepest bin at 192 m.

During Hurricane Igor in 2010, the OFP mooring was equipped with a two-dimensional acoustical current meter (FASI ACM 2D, Falmouth Scientific, Falmouth MA) at 750 m depth. The instrument sampled data every 2 hours, with duplicate measurements spaced 5 minutes apart.

Additional temperature profiles were obtained from CTD deployments at the BATS site collected pre (25 Aug 2003) and post Fabian (19 Sep 2003). Details of the BATS methodologies are provided in Steinberg et al. (2001).

3.3. Particle Fluxes

The OFP mooring and sample collection methods are provided in Conte et al. (2001). The OFP mooring uses conical Parflux sediment traps (McLane Research Laboratories, Falmouth MA, USA) having a 0.5 m^2 sampling area. Traps are deployed at 500, 1,500 and 3,200 m depths and continuously collect the sinking particle flux at an approximate biweekly resolution. Trap cups are filled with deep seawater brine (41 ppt) poisoned with ultra-trace metal purity $HgCl_2$ (200 mg L^{-1}) to prevent organic matter degradation. Before deployment, trap cups are filled in a laminar flow hood with a trace metal clean brine (41 ppt), prepared from seawater collected at 3,000 m depth using trace-metal clean Go-Flo bottles, poisoned with ultra-purity mercuric chloride (200 mg L^{-1}) to arrest bacterial activity. Process and deployment blanks are collected during each deployment to assess potential contamination.

3.4. Analytical Methods

OFP sample processing: Sample processing protocols are described in Conte et al. (2001, 2003, 2019). Prior to quantitative sample splitting, >1,000 μm-sized material is transferred to a pre-weighed Petri dish for photography, removal of swimmers, and dried at 55°C for mass determination. The remaining, <1000 μm material is split using a McLane rotary splitter (McLane Research Laboratories, Falmouth, MA, USA). Three subsamples are designated for organic analysis and one for trace elemental analysis. The remaining subsamples (60%) are recombined and fractionated into 500–1,000 μm, 125–500 μm, and <125 μm size fractions. For Hurricanes Fabian (25 Aug-8Sep 2003) and Igor (13–28 Sep, 28 Sep −12 Oct 2010) samples, the <125 μm fraction was divided into additional size fractions to better characterize the hurricane sediment plumes. The 63–125 μm ("fine sand") and 37–63 μm ("coarse silt") fractions were separated using stainless-steel sieves. The 4–37 μm ("medium-fine silt") fraction was concentrated by centrifuging 7 min at 1,000 rpm, and the supernatant containing the <4 μm ("clay") fraction was concentrated by centrifuging 10 min at 3,000 rpm (modified from Pedrosa-Pàmies et al., 2013). We note that for these detrital carbonate sediments the standard nomenclature commonly used for these fractions is an operational definition only.

The larger size fractions (>125 μm) were quantitatively photographed (described below), dried at 55°C and weighed to the nearest 0.01 mg. <125 μm size fraction was freeze-dried and weighed. Mass flux was calculated from combined weights of all size fractions.

Microscopy: Microscopy details are provided in Shatova et al. (2012). All >125 μm size fractions were quantitatively photographed using a Zeiss Stemi SV-11 stereomicroscope with an Olympus DP73 camera (17.3 MP). The sample dish was placed atop blue optical glass with a laser-etched cm^2 grid (Schott IMERA 4218, Schott USA). Magnification, photographic, and illumination settings were tightly controlled to maintain image uniformity.

Scanning Electron Microscopy (SEM) of larger size fractions of samples collected just after hurricane passage was conducted using a Zeiss Supra 40VP instrument. Samples were coated with 5 nm of Pt before SEM imaging.

Carbonate analyses: Carbonate analyses were performed using a Coulometrics model 5011 coulometer (UIC Inc.) equipped with a System 140 module for inorganic carbon determination. Analytical uncertainty is <1.8% based on repeated measurements of flux material working standards. Carbonate $\delta^{13}C$ and $\delta^{18}O$ were analyzed using a Finnigan MAT252 mass spectrometer following the procedure of Ostermann and Curry (2000). Analytical precision was ±0.04 for $\delta^{18}O$ and ±0.05 for $\delta^{13}C$ based on the reproducibility of the internal WHOI Atlantis II coral standard. Bulk and isotopic analyses are made on the <125 μm size fraction and converted to total flux by assuming that the total mass composition approximates that of the <125 μm fraction which comprises most of the mass.

X-Ray Diffraction (XRD) analysis was conducted for the Fabian plume material collected in the 1,500 m OFP trap. XRD was performed using a Scintag PAD V powder X-ray diffractometer at the School of Ocean and Earth Science and Technology at the University of Hawaii at Manoa. The X-ray source was a copper anode tube emitting X-rays at 1.540562 Å for $\kappa\alpha_1$. The detector was a solid-state Ge detector. Data measurements were made during two scans, the first covering 2°–60° 2θ at a rate of 1°2θ/minute and the second scan focusing on the main Mg-calcite peak between 28° and 32° 2θ at a rate of 0.1°2θ/minute. The average Mg-calcite composition was calculated from the *d*-spacing offset of the calcite peak owing to incorporation of Mg following Bischoff (1985): $d_{104} = -0.29166\ (X_{MgCO3}) + 3.0350$, where d_{104} is the d-value of the Mg-calcite peak obtained from the slow scan and X_{MgCO3} is the mol fraction $MgCO_3$. The last term (3.0350) is the d-spacing of the main peak of pure calcite.

A semi-quantitative estimate of the relative mineralogical composition aragonite, calcite and Mg-calcite in the trap sample was calculated by integration of peak areas using processing software JADE (Materials Data Inc., MDI). The aragonite content was calculated from a relationship derived by Sabine (1992): $\%\ Arag = 97.711 - 25.145e^{(-0.455\times PAR)} - 68.791\times e^{(-4.952\times PAR)}$, where PAR is the peak area ratio of aragonite (peak 111) to calcite (peak 104). The relative composition of Mg-calcite and calcite was calculated directly from the PAR of these mineral phases.

Organic carbon analyses: Particulate organic carbon (POC) and nitrogen (N) concentrations and stable isotopic composition were analyzed using a Europa 20-20 CF-IRMS interfaced with the Europa ANCA-SL elemental

analyzer. Before analysis, carbonates were removed by pre-treatment with 4% sulfurous acid using a modified Verardo et al. (1990) method. Analytical uncertainty is <0.18% based on repeated measurements of flux material working standards.

Elemental analysis: Elemental analyses were made on the total <1,000 μm material using a fusion-Inductively Coupled Plasma Mass Spectrometry (ICPMS) method developed for multi-elemental analysis of flux material (Huang et al., 2007). Briefly, the dried sample (4–6 mg) is fused with high purity lithium metaborate ($LiBO_2$) flux at 1,000°C in a dedicated combustion furnace, using a sample to $LiBO_2$ flux ratio of 1:2.5. The fused sample bead was dissolved in 1M HNO_3 for ICPMS analysis. Samples were analyzed on a Finnigan Element 2 ICPMS at the Woods Hole Oceanographic ICPMS Facility.

Lithogenic concentration was estimated from Si and Al concentrations, assuming that the Al flux was carried mainly by lithogenic particles whose composition approximates that of pelagic clay sediments (25% Si and 8.4% Al, Li and Schoonmaker, 2003):

$$[\text{Lithogenic}] = \frac{[\text{Al}]}{0.084} \tag{1}$$

Biogenic Si was estimated by subtracting the lithogenic Si from the total Si and converted to opal assuming an opal water content of $SiO_2{\cdot}0.4H_2O$ (Mortlock & Froelich, 1989).

Element enrichment factors (EF) were calculated relative to the average concentration of upper continental crust (UCC) normalized to aluminum (Al) (Rudnick & Gao, 2003):

$$\text{EF} = \frac{\frac{[X]_{\text{sample}}}{[Al]_{\text{sample}}}}{\frac{[X]_{\text{UCC}}}{[Al]_{\text{UCC}}}} \tag{2}$$

Phosphorus is the sum of particulate P (measured by ICPMS) and dissolved P lost into the supernatant during sample collection. Dissolved P was analyzed using a Lachat autosampler (QuikChem FIA^+ 8000 series, XYZ Autosampler 500 Series). Typical sample c.v. is ∼2%.

Lipid analysis: Lipid analytical methods are detailed in Pedrosa-Pàmies et al. (2018). An internal standard mixture (n-$C_{21:0}$ fatty alcohol, n-$C_{23:0}$ fatty acid, 5α-cholestane and n-$C_{36:0}$ alkane) was added to samples prior to lipid extraction. Lipids are ultrasonically extracted using 2:1 $CHCl_3$-MeOH, transesterified using anhydrous 10% methanolic HCl (55°C, 12 hr) (Christie, 1982), and trimethylsilylated using pyridine and N,O-Bis (trimethylsilyl) trifluoroacetamide + 1% Trimethylchlorosilane (BSTFA + 1% TMCS). The transesterified TMS derivatives were analyzed on an Agilent 7890A GC coupled to a 5975C MS equipped with triple-axis MS and FID detectors. A Varian CPSil 5CB column (60 m × 0.25 mm diameter x 0.25 μm film thickness) was used for compound separation. Compounds were identified by mass spectra and quantified from their FID response relative to the internal standard. Analytical uncertainties range between 4% and 11%, based upon repeated analyses of samples having similar lipid composition (Pedrosa-Pàmies et al., 2018).

4. Results

4.1. Hurricane Fabian 2003

4.1.1. Hurricane Characteristics and Ocean Response

Hurricane Fabian passed through the region as a Category 3 storm with maximum sustained winds of 54 m s^{-1} and a central pressure near 950 mb. Fabian tracked 9° northward at 8.8 m s^{-1}. Its eyewall was approximately 26 km west of Bermuda and 115 km west of the OFP mooring at 1800 UTC on Sep 5. Fabian generated 9 m surface waves and a 3 m storm surge along Bermuda's south shore (Pasch et al., 2003). The 8-day composite SST shows a cool swath about 200 km wide centered about 140 km to the right of the hurricane track and over the OFP site, with the SST ∼3°C lower than the surrounding waters (Figure 2a). Sea surface height (SSH) did not reveal any strong mesoscale eddy features during Fabian (Figure 2b).

Fabian caused platform-wide sediment resuspension, seen in a satellite image the day after Fabian (Figure 2c). In the image, the platform rim is revealed by the distinct change in water color from cyan, corresponding to water

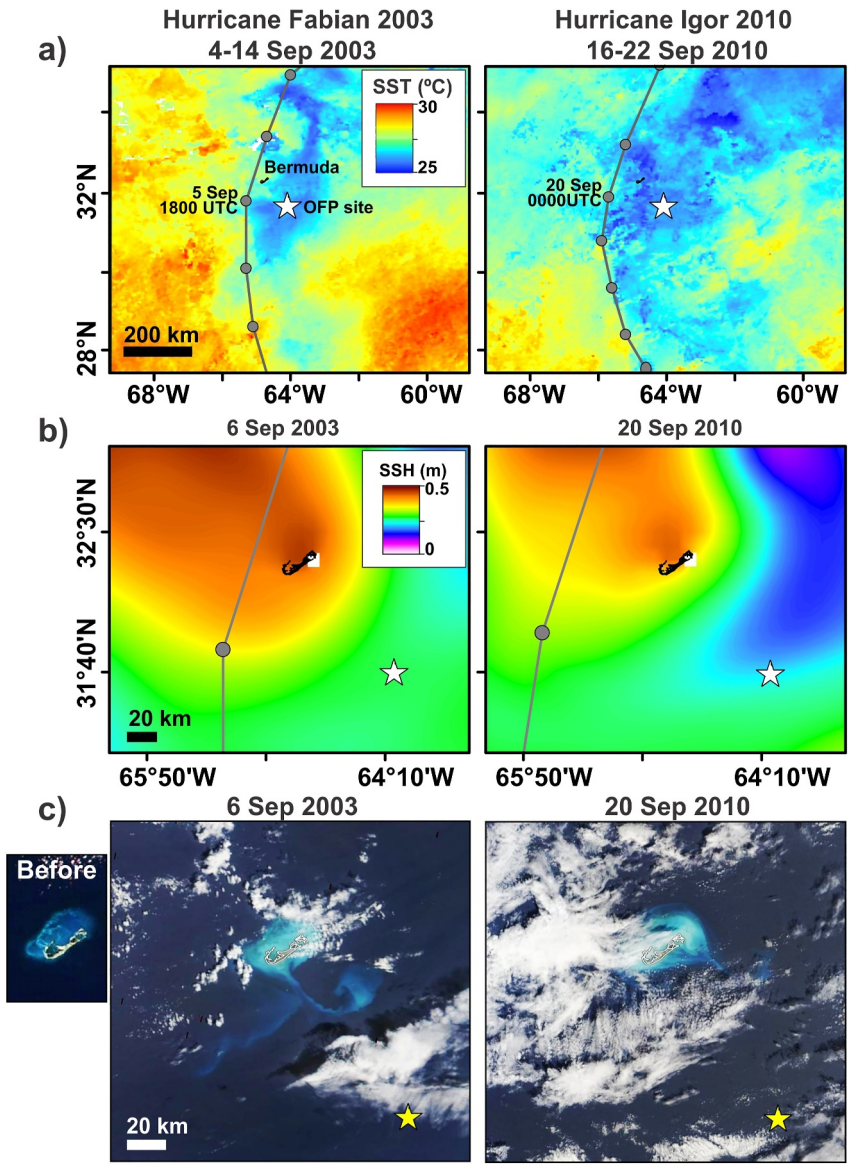

Figure 2. (a) Sea surface temperature (SST, °C) and (b) Sea surface height (SSH, m) after the passage of hurricanes Fabian 2003 and Igor 2010. The stars indicate the location of the OFP site, and the lines/circles correspond to the hurricane tracks. (c) Satellite imagery taken the day after hurricanes passed Bermuda showing surface sediment plumes. The inset shows a typical non-hurricane disturbed satellite image of the Bermuda Platform.

rich in resuspended platform sediments, to dark blue. A surface sediment plume extends offshore south of the platform, with one filament stretching toward the OFP site.

The BTM mooring provided in situ data as Fabian passed. Black and Dickey (2008) describe the upper ocean response. SST decreased ~3.5°C during Fabian's closest approach to the BTM (Sept 5), consistent with satellite data. The mixed layer deepened from 20 to 50 m depth. Coincident warming between 17 and 92 m depths indicated entrainment of thermocline waters. Surface currents > 160 cm s^{-1} were measured on Sep 6. Currents did not drop below 30 cm s^{-1} until Sep 15, approximately 11 inertial periods later (inertial period = 22.8 hr). Vertical velocities in the mixed layer were ~10^{-4} m s^{-1}, resulting in rapid downmixing to >130 m depth (Black & Dickey, 2008).

Temperature oscillations measured by sensors on the BTM mooring evidenced generation of strong near-inertial, sub- and super-inertial waves down to depths of at least 751 m, the deepest sensor on the BTM (Figure 3a). The

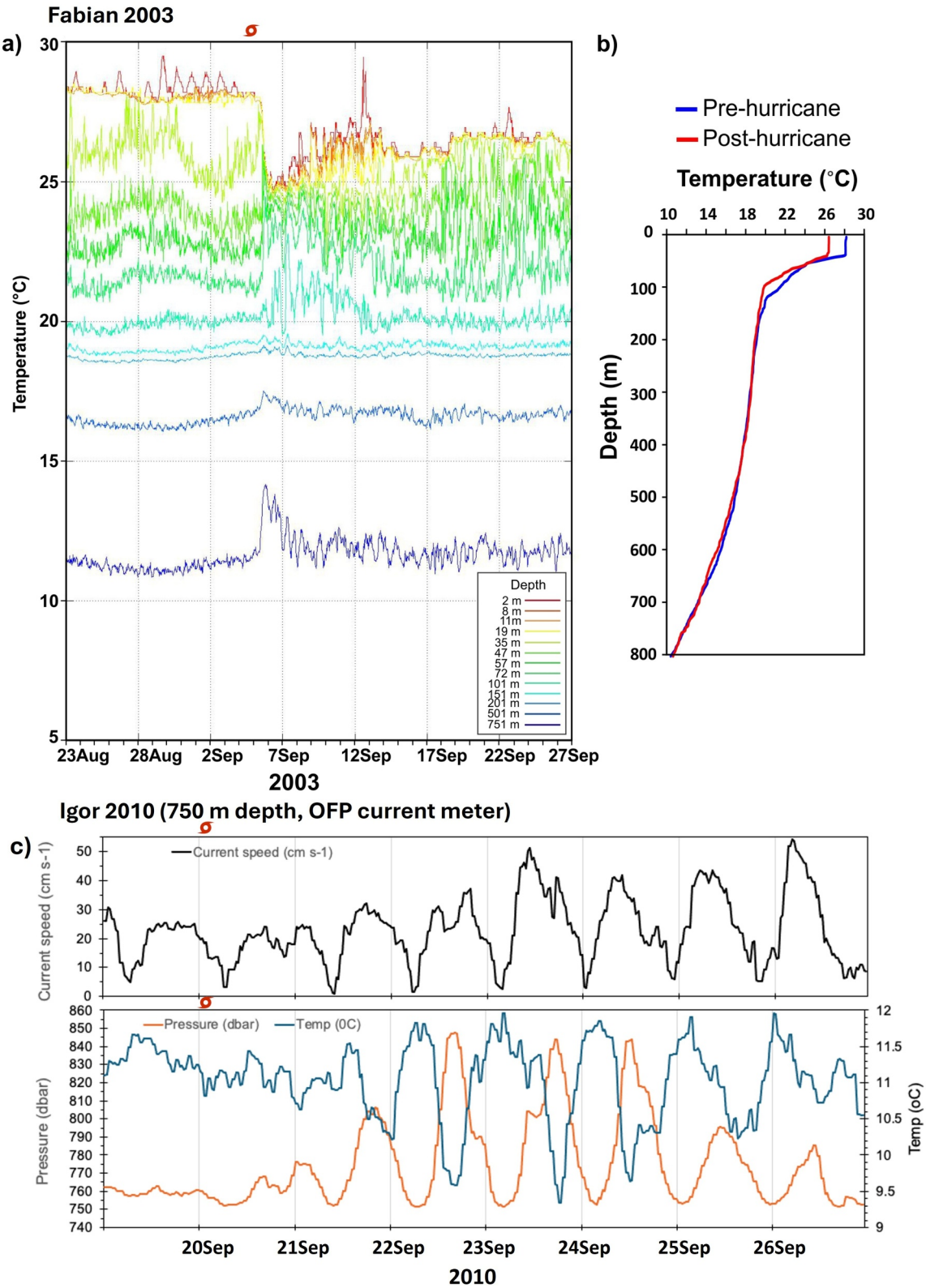

Figure 3. (a) Temperature records from sensors on the BTM mooring as Hurricane Fabian passed through (unpublished data, T. Dickey et al.). (b) Temperature structure of the water column pre (25 Aug 2003) and post (19 Sep 2003) Fabian passage. (c) Current (top) and pressure (bottom) data collected at 750 m before and after Igor passage through Bermuda (20 Sep 2010). Red hurricane symbols indicate timing of hurricane closest approach.

BTM measured temperature profile of the upper 800 m water column during Fabian is compared with the pre-Fabian temperature profile to estimate wave displacements at the different depths (Figure 3b). Oscillations at 100 m depth recorded a wave displacement of ~7 m at the base of the seasonal thermocline. Small temperature oscillations within the ~18°C subtropical mode water (150 and 201 m depth) revealed wave oscillations were in phase with those in the seasonal thermocline.

Importantly, very large temperature oscillations in the deep water column indicated that the wave energy generated by Fabian propagated downward at least 751 m depth (Figure 3a). Notably, a large abrupt temperature increase was observed at both 500 and 751 m depths on Sep 5. We calculated wave isopycnal displacements (η) using the formula of Black and Dickey (2008):

$$\eta = \frac{\Delta T}{dT/dz} \tag{3}$$

where ΔT is the temperature displacement at 501 and 751 m for the oscillation peak (0.8 and 2.1°C, respectively) and dT/dz is the temperature gradient of the depth interval bracketing the thermistor depths, measured by the CTD cast eight days prior to Fabian (Figure 3b). Between 650 and 800 m the temperature gradient dT/dz was 0.026°C m^{-1}, resulting in an initial isopycnal displacement of 80 m at 751 m depth. Between 450 and 550 m the temperature gradient dT/dz was 0.0108°C m^{-1}, resulting in a comparable initial isopycnal displacement of 75 m at 501 m. Temperature oscillations remained above baseline until the end of the record on Sep 27.

We estimated vertical velocities (w) at 501 and 751 m depths using the formula of Black and Dickey (2008):

$$w = \frac{4\eta}{IP} \tag{4}$$

where η is the isopycnal displacement and IP is the inertial period (22.8 hr). The estimated magnitude of vertical velocities at 501 and 751 m were similar and on the order of 4×10^{-3} m s^{-1} for the initial deep internal waves arriving at the BTM site on Sep 5.

Although we do not have direct evidence of interactions of these large deep internal waves with the Pedestal slope, models and observational studies (e.g., Alford et al., 2012; Keen & Allen, 2000; H. van Haren et al., 2020) have shown downward energy propagation by hurricanes producing deep internal waves of a similar magnitude deeper than 500 m depth, which then interact with sloping boundaries to resuspend and transport large plumes of sediments.

4.1.2. Particle Export to the Deep: Bulk Fluxes and Plume Carbonate Composition

Following Fabian, Total Mass Flux (TMF) increased 9-fold at 500 m, 16-fold at 1,500 m, and 4-fold at 3,200 m (Figure 4a, and Table 1). Notably, the TMFs at depths of 1,500 and 3,200 m were the highest measured at the OFP site since 1978. The TMF at 1,500 m depth during the 2 weeks after Fabian was equivalent to ~50% of the annual TMF at this depth (average 12.7 g m^{-2} y^{-1}).

The plumes intercepted by the traps contained primarily fine-grained (<125 μm) particles (Table 1; Figure S2 in Supporting Information S1): 91% of TMF at 500 m, 96% at 1,500 m and 94% at 3,200 m depths (Table 1), significantly higher than that in the typical oceanic flux (annual averages: 51% at 500 m, 77% at 1,500 m and 81% at 3,200 m).

Further grain size separation of the <125 μm particles was conducted for the samples collected during the hurricane plume peak (Figure 5). The fine-grained size distribution of the plume at 500 m depth was 35.7% 63–125 μm size particles ("fine sand"), 20.2% 37–63 μm ("coarse silt"), 35.1% 4–37 μm ("medium-fine silt"), and 0.5% < 4 μm ("clay") (note that the size category definitions are operational only.) The 1,500 m and 3,200 m plumes consisted of finer particles, with "fine silt"-sized particles approximately 4% and 8% more abundant, respectively. "Clay"-sized particles were also more abundant in the 1,500 m and 3,200 m plumes by 0.1% and 0.4%, respectively (Figure 5).

The hurricane plumes were overwhelmingly composed of carbonates (88.2% at 500 m, 92.8% at 1,500 m, and 73.5% at 3,200 m) (Table 1). Relative to pre-Fabian conditions, carbonate fluxes increased 15-fold at 500 m, 32-

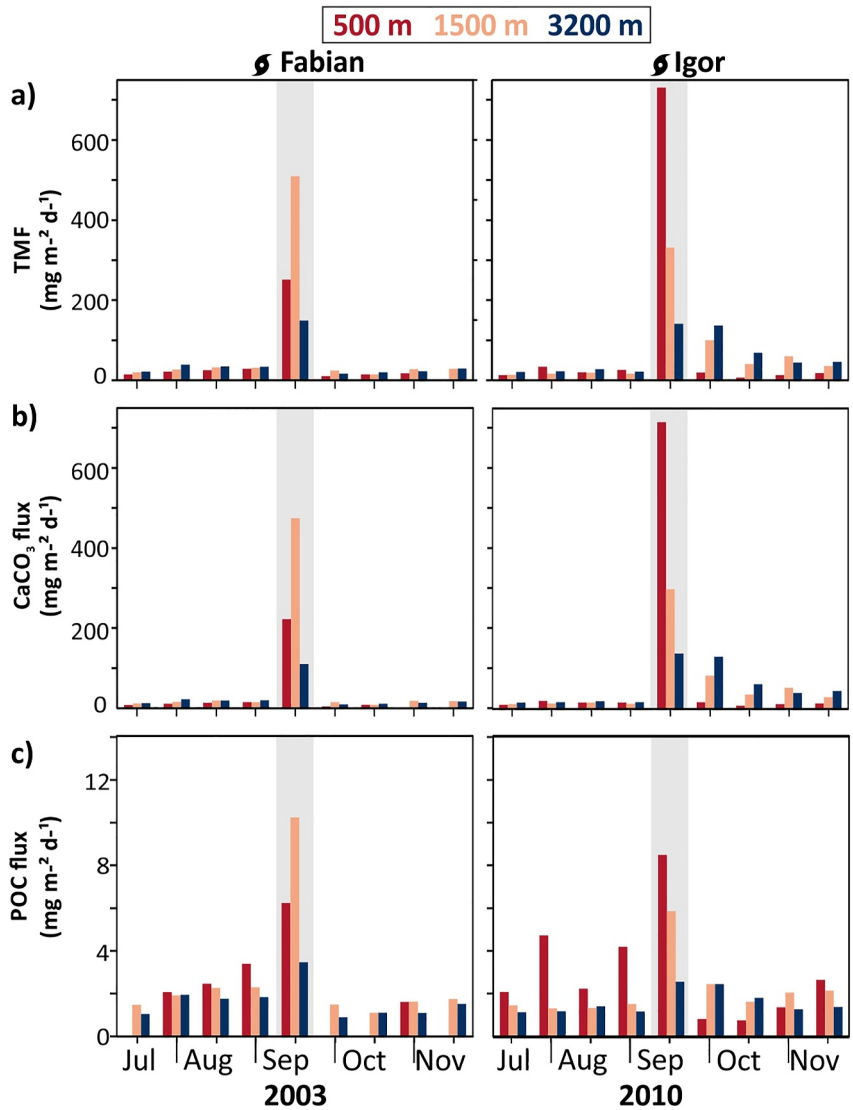

Figure 4. (a) Total mass flux (TMF), and (b) carbonate ($CaCO_3$) and (c) particulate organic carbon (POC) fluxes at 500 m (red), 1,500 m (orange) and 3,200 m (dark blue). Samples collected immediately after the hurricanes are shaded gray.

fold at 1,500 m, and 6-fold at 3,200 m (Figure 4b). During the two-week period after Fabian, carbonate fluxes at 1,500 m and 3,200 m depths were equivalent to ~ 91% and ~20% of the annual carbonate flux at these depths, respectively (7.8 g CaCO3 m^{-2} y^{-1} 1,500 m avg. 1984–2022, 8.1 g CaCO3 m^{-2} y^{-1} 3,200 m avg. 1978–2022).

Microscopic analysis of the larger size fractions of plume material (>125 μm) showed the dominance of platform reef-sourced carbonate debris (Figure S3 in Supporting Information S1). Many fecal pellets and amorphous particle aggregates contained abundant quantities of shallow-water detrital carbonates such as coral and coralline algae fragments, as well as typical pelagic biogenic carbonates such as coccoliths, foraminiferal and pteropod shell fragments.

Carbonate stable isotopes, elemental ratios, and carbonate mineral composition provided further evidence of the Pedestal carbonate origin of the hurricane plumes (Figure 6). Prior to Fabian's passage, the background carbonate $\delta^{13}C$ of the particle flux measured 0.63‰ at 500 m depth, 0.23‰ at 1,500 m depth, and −0.29‰ at 3,200 m depth, and the background carbonate $\delta^{18}O$ measured 0.15, 0.09‰, −0.02‰, at 500 m depth, 1,500 m depth, at 3,200 m depth, respectively. These values are typical of that of open ocean pelagic calcifiers at the OFP site (Anand et al., 2003; Babila et al., 2014; Deuser et al., 1981; Gray, 2019; Jasper & Deuser, 1993; Juranek et al., 2003; Steiger, 2019).

Table 1
Total Mass Flux (TMF) and Fluxes of Major Components in the Sample Collected Prior to Hurricane Passage and in the Plume Sampled After the Hurricane Passed Over

Depth (m)		TMF (mg m^{-2} d^{-1})	<125 μm (%)	$CaCO_3$ flux (mg m^{-2} d^{-1})	$CaCO_3$ (%)	POC flux (mg m^{-2} d^{-1})	POC (%)	Lipid content in total POC (%)	P flux (mg m^{-2} d^{-1})	Opal flux (mg m^{-2} d^{-1})	Opal (%)	Lithogenic flux (mg m^{-2} d^{-1})	Lithogenic (%)
Fabian													
500	pre-hurricane	26.6	66.9	13.6	60.9	2.2	8.3	5.2	137.5	2.3	8.6	3.2	12.3
500	hurricane peak	251.4	91.4	221.7	88.2	4.7	2.5	2.0	323.9	1.5	0.6	2.6	1.0
500	*flux ratio	9.4		16.3		2.1		0.4	2.4	0.7		0.8	
1,500	pre-hurricane	31.5	84.1	16.6	52.6	2.3	7.2	4.9	59.3	3.0	9.6	3.4	10.7
1,500	hurricane peak	510.0	95.8	473.3	92.8	10.2	2.0	1.2	310.3	2.4	0.5	11.2	2.2
1,500	*flux ratio	16.2		28.6		4.5		0.2	5.2	0.8		3.3	
3,200	pre-hurricane	34.4	82.4	18.9	54.6	1.8	5.2	1.0	25.2	4.4	12.8	6.6	19.2
3,200	hurricane peak	149.1	93.5	109.6	73.5	3.5	2.3	1.3	91.5	7.0	4.7	ND	ND
3,200	*flux ratio	4.3		5.8		1.9		1.3	3.6	1.6		ND	
Igor													
500	pre-hurricane	26.1	76.3	14.6	67.3	2.4	9.1	7.1	176.6	1.2	5.4	1.9	8.4
500	hurricane peak	732.2	95.3	716.9	97.9	6.4	1.2	2.1	463.5	6.4	0.9	3.5	0.5
500	*flux ratio	28.0		49.2		2.7		0.3	2.6	5.1		1.8	
1,500	pre-hurricane	20.7	75.5	12.9	62.4	1.4	6.9	18.8	53.2	3.0	14.8	3.1	15.0
1,500	hurricane peak	333.9	90.1	298.7	89.4	5.8	1.8	5.2	201.9	9.8	2.9	6.0	1.8
1,500	*flux ratio	16.2		23.1		4.1		0.3	3.8	3.3		1.9	
3,200	pre-hurricane	27.7	77.2	15.3	59.7	1.3	4.6	2.4	25.0	3.0	10.6	5.6	19.8
3,200	hurricane peak	143.9	86.7	137.2	95.3	2.5	1.8	1.8	76.9	2.5	1.7	5.7	4.0
3,200	*flux ratio	5.2		9.0		2.0		0.8	3.1	0.8		1.0	

Note. For Hurricane Fabian, the pre-hurricane sampling period was 11 Aug–8 Sep 2003 and plume sampling period was 8–23 Sep 2003. For Hurricane Igor 2010, the pre-hurricane sampling period was 14 Aug–23 Sep 2010 and plume sampling period was 13–28 Sep 2010. *Flux ratio is the ratio post-hurricane/pre-hurricane.

Following Fabian, these values increased to approximately 1.5‰ at all depths. Carbonate $\delta^{18}O$ decreased from 0.15‰ to −0.34‰ at 500 m depth, 0.09‰ to −0.59‰ at 1,500 m depth, and −0.02‰ to −0.27‰ at 3,200 m depth. Carbonate $\delta^{13}C$ increased from 0.63 to 1.64‰ at 500 m depth, 0.23–1.49‰ at 1,500 m depth, and −0.29–1.40‰ at 3,200 m depth. The isotopic composition of the plumes lies within the range of $\delta^{18}O$ and $\delta^{13}C$ of neritic biogenic carbonate production (approx. −1 to +3‰ and 0 to +5‰, respectively (Higgins et al., 2018; Swart et al., 2009)).

Extreme increases in the molar Mg/Ca, Sr/Ca and Mg/Sr elemental ratios in the Fabian plume (Figure 6) also evidenced the greatly increased percentages of aragonite and high-Mg calcites in the plume relative to the typical pelagic carbonate flux at the OFP site (Conte et al., 2019; Huang & Conte, 2009). The carbonate elemental

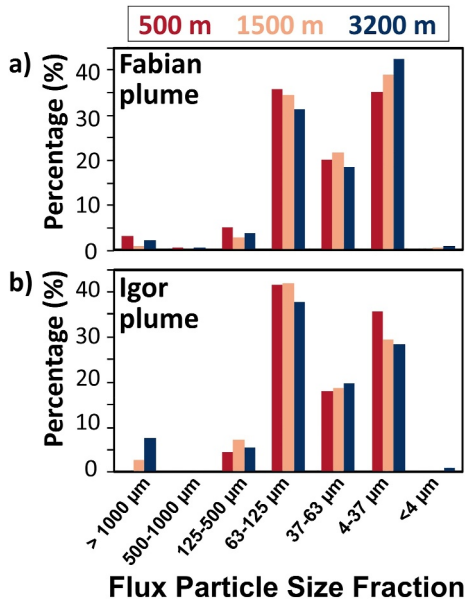

Figure 5. Percentage of particle size fractions (>1,000 µm, 500–1,000 µm, 125–500 µm, 63–125 µm, 37–63 µm, 4–37 µm, and <4 µm) in the Fabian (a) and Igor (b) hurricane plumes collected at 500 m (red), 1,500 m (orange), 3,200 m (blue).

composition of the plume is compared to background pelagic carbonates in the sinking flux prior to the hurricane event (Figure S4 in Supporting Information S1). The Mg/Ca ratio in the pelagic flux prior to Fabian ranged from 0.2 to 0.5, within the range of pelagic calcifying organisms (e.g., Anand et al., 2003; Stoll et al., 2007) and consistent with the dominance of calcite in the particle flux (Fabry & Deuser, 1991; Huang & Conte, 2009). During the Fabian plume event, the Mg/Ca molar ratio increased 2-fold at 500 m depth, 3.4-fold at 1,500 m depth, and 2.0-fold at 3,200 m depth. Similarly, the Sr/Ca molar ratio in the plume increased 1.6-fold at 500 m depth, 1.7-fold at 1,500 m depth, and 1.5-fold at 3,200 m depth. The Mg/Sr molar ratio increased 1.3-fold at 500 m, 1.9-fold at 1,500 m, and 1.4-fold at 3,200 m depths (Figure 6). These observations are consistent with a dominance of aragonite and high-Mg calcites in the Fabian plume.

XRD analysis of carbonates in the 1,500 m depth Fabian plume supported the elemental data. XRD-based estimates of the relative mineralogical composition of aragonite, Mg-calcite and calcite in the Fabian plume were 43%, 46%, 11% respectively. This relative percentage of carbonate minerals is consistent with reef-sourced biogenic detrital carbonates characterizing the Bermuda Pedestal sediments, which averaged between 40% and 50% of high Mg-calcite at depths ranging from 1,000 m to 2,000 m (Lavoie & Matthews, 1983). In contrast, the pelagic carbonate flux is dominated by low Mg-calcite synthesized mainly by the coccolithophores and forams (Morse & Mackenzie, 1990), with lesser amounts of aragonite synthesized mainly by pteropods and minimal production of high-Mg calcites (Fabry & Deuser, 1991). The semi-quantitative estimate of the relative carbonate percentage of the Mg-calcite phase averaged 14.1 mol% $MgCO_3$. This is within the typical 13–15 mol% $MgCO_3$ of the average Mg-calcite composition of shallow (<20 m) sediments (Pickett & Andersson, 2015; Andersson, unpublished), and similar to the average mol% $MgCO_3$ measured in mid slope sediments (11.5–12.5 mol % $MgCO_3$, 1,475–2,800 m) of the Bermuda Pedestal (Berner et al., 1976).

In contrast to the massive increase in the carbonate flux, opal fluxes did not increase significantly during the Fabian plume event (Table 1).

Fluxes of P and lithogenic elements increased several-fold during the Fabian plume event, indicating significant transport of phosphorus and lithogenic materials that had accumulated on the Pedestal (Table 1). P fluxes increased ~2-fold at 500 m, ~5-fold at 1,500 m and ~4-fold at 3,200 m. The lithogenic flux at 1,500 m depth increased 3.3-fold, partly due to the high lithogenic percentage in the plume material at this depth.

Pollutant elements (e.g., Pb, V, Cd, Zn, Cu) also increased significantly during the Fabian plume event (Table 2). Pb fluxes increased ~6-fold at 500 m, ~12-fold at 1,500 m, and ~2-fold at 3,200 m depth, and V fluxes increased ~3-fold at 1,500 m. Cd fluxes increased ~3-fold at 500 m, ~21-fold at 1,500 m, and ~4-fold at 3,200 m, and Zn fluxes increased ~3-fold at 500 m, ~12-fold at 1,500 m, and ~2-fold at 3,200 m. Cu fluxes also increased ~2-fold at 500 m, ~6 fold at 1,500 m, and ~2-fold at 3,200 m. Notably, the Pb flux at 1,500 m after Fabian was the highest observed in the entire OFP elemental time-series (2001–2015), and was equivalent of ~50% of the annual Pb flux at the OFP site (Conte et al., 2019).

POC fluxes also increased during the Fabian plume event (Figure 4c, Table 1). POC fluxes were ~2-fold higher at 500 and 3,200 m and ~5-fold higher at 1,500 m depth. The lipid percentage of the POC at 500 and 1,500 m depths decreased from ~5%–2% and to ~1%, respectively, indicating the plume contained more refractory POC, further evidence of a sedimentary origin. The lipid percentage of the POC did not increase at 3,200 m depth, reflecting the low contribution of plume POC to the TMF.

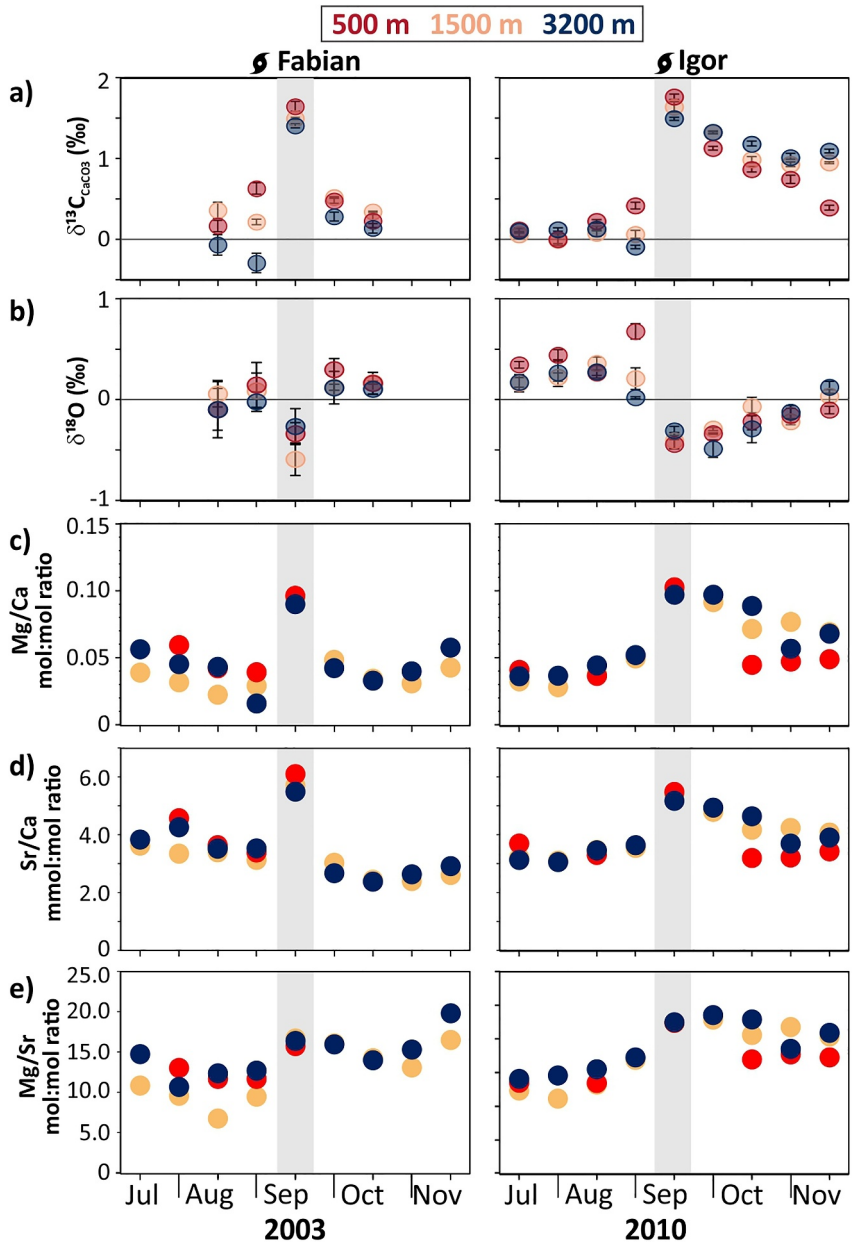

Figure 6. Carbonate stable isotope and molar elemental ratios in the flux at 500 m (red), 1,500 m (orange) and 3,200 m (blue) prior to and after hurricanes Fabian and Igor. The flux samples collected immediately after the hurricanes are shaded gray. (a) $\delta^{13}C$, (b) $\delta^{18}O$, (c) Mg/Ca, (d) Sr/Ca, and (e) Mg/Sr.

4.1.3. Fabian Sediment Plume Composition: Non-carbonate Components

4.1.3.1. Element Enrichments and Particle Size Associations

The enrichment of non-carbonate elements in the plumes was estimated by comparing the enrichment factor (EF) of element X in the peak plume flux to the median EF in the particle flux (Conte et al., 2019):

$$\text{EF hurricane sediment plume} = \frac{[\text{X EF}]_{\text{hurricane peak flux}}}{[\text{X EF}]_{\text{OFP median flux}}} \quad (5)$$

The plumes intercepted at all depths were consistently enriched in the pollutant element Pb and depleted in the lithogenic element Ti. Otherwise, each depth exhibited a distinctive elemental signature (Figure 7). At 500 m

Table 2
Element Fluxes ($\mu g\ m^{-2}\ d^{-1}$) Prior to Hurricane Passage and in the Hurricane Plume

Depth (m)		Al	Sc	Ti	Cu	Ni	P	Zn	Cd	Fe	Mn	Ba	Co	Pb	V
Fabian															
500	pre-hurricane flux	272.6	0.03	12.1	1.28	0.55	142.96	3.37	0.05	152.43	11.9	18.47	0.14	3.45	0.41
500	hurricane peak flux	216.8	0.03	ND	3.08	1.36	349.2	9.23	0.14	161.4	19.9	14.3	0.14	17.8	0.36
500	*flux ratio	0.80	0.84	ND	2.41	2.45	2.44	2.74	3.04	1.06	1.67	0.77	0.93	5.15	0.88
500	** plume flux	-	-	-	1.80	0.8	206.3	5.86	0.10	8.98	8.00	-	-	14.3	-
500	** plume conc.	-	-	-	8.01	3.58	917.6	26.1	0.43	40.0	35.6	-	-	63.7	-
1,500	pre-hurricane flux	283.0	0.03	9.40	1.92	0.88	63.5	1.72	0.03	166.9	26.4	23.6	0.32	3.55	0.52
1,500	hurricane peak flux	939.4	0.13	17.3	11.2	3.86	339.1	25.4	0.45	589.6	84.1	82.6	0.79	34.8	1.86
1,500	*flux ratio	3.32	3.68	1.84	5.84	4.36	5.34	14.8	16.81	3.53	3.19	3.50	2.47	9.82	3.60
1,500	** plume flux	656.4	0.09	7.86	9.31	2.97	275.6	23.7	0.42	422.7	57.7	59.0	0.47	31.3	1.35
1,500	** plume conc.	1,371.7	0.19	16.4	19.5	6.21	576.0	49.5	0.88	883.4	120.5	123.2	0.99	65.4	2.82
3,200	pre-hurricane flux	553.1	0.07	21.9	3.01	1.73	25.2	2.73	0.02	326.4	44.7	30.0	0.54	4.5	1.11
3,200	hurricane peak flux	587.4	0.09	11.6	4.68	1.58	91.5	4.8	0.06	346.8	41.1	45.7	0.42	9.93	1.16
3,200	*flux ratio	1.06	1.22	0.53	1.56	0.91	3.64	1.76	3.23	1.06	0.92	1.53	0.78	2.21	1.04
3,200	** plume flux	34.2	0.02	-	1.68	-	66.4	2.07	0.04	20.5	-	15.7	-	5.45	0.05
3,200	** plume conc.	298.5	0.14	-	14.6	-	578.7	18.1	0.38	178.5	-	137.2	-	47.5	0.43
Igor															
500	pre-hurricane flux	160.4	0.02	8.42	1.19	1.49	176.6	3.19	0.09	157.9	ND	15.4	0.12	1.45	0.92
500	hurricane peak flux	291.0	0.22	17.8	1.77	3.37	463.5	7.87	0.15	913.0	32.5	68.7	0.42	9.19	2.27
500	*flux ratio	1.81	9.12	2.12	1.49	2.27	2.62	2.47	1.74	5.78	ND	4.46	3.46	6.34	2.48
500	**plume flux	130.5	0.19	9.40	0.59	1.88	286.9	4.68	0.06	755.2	ND	53.3	0.30	7.74	1.35
500	** plume conc.	184.9	0.27	13.3	0.83	2.66	406.3	6.62	0.09	1,069.5	ND	75.5	0.42	11.0	1.92
1,500	pre-hurricane flux	262.1	0.04	12.9	1.48	0.72	54.0	1.46	0.02	178.8	20.9	22.1	0.22	1.86	0.61
1,500	hurricane peak flux	502.2	0.16	20.5	2.23	2.11	190.5	5.81	0.09	464.5	54.1	53.2	0.57	7.62	1.47
1,500	*flux ratio	1.92	3.96	1.59	1.50	2.92	3.53	3.98	5.52	2.60	2.59	2.40	2.51	4.09	2.41
1,500	** plume flux	240.1	0.12	7.56	0.74	1.39	136.5	4.36	0.08	285.7	33.2	31.1	0.34	5.76	0.86
1,500	** plume conc.	766.6	0.38	24.1	2.37	4.43	435.8	13.9	0.25	912.3	106.0	99.2	1.09	18.4	2.74
3,200	pre-hurricane flux	467.1	0.07	22.8	2.57	1.02	25.0	1.28	0.03	314.4	32.1	29.5	0.31	2.64	1.11
3,200	hurricane peak flux	480.8	0.11	19.8	2.36	1.17	76.9	1.37	0.04	375.1	39.1	65.6	0.39	6.39	1.21
3,200	*flux ratio	1.03	1.58	0.87	0.92	1.15	3.08	1.07	1.42	1.19	1.22	2.22	1.26	2.42	1.09
3,200	** plume flux	13.7	0.04	-	-	0.15	51.9	0.09	0.01	60.8	6.98	36.0	0.08	3.75	0.10
3,200	** plume conc.	117.6	0.34	-	-	1.31	446.3	0.81	0.09	522.8	60.1	309.9	0.69	32.2	0.84

Note. For Hurricane Fabian, the pre-hurricane sampling period was 11 Aug–8 Sep 2003 and plume sampling period was 8–23 Sep 2003. For Hurricane Igor 2010, the pre-hurricane sampling period was 14 Aug–23 Sep 2010 and the plume sampling period was 13–28 Sep 2010. *Flux ratio is the plume/pre-hurricane ratio. The plume elemental fluxes and concentrations (mg kg^{-1}) were estimated by subtracting the pre-hurricane flux from the plume flux. "-" indicates element flux was not elevated in the plume. ND = no data.

depth, the plume was highly enriched in Mn, Cu and Zn and depleted in P, Ba and Co. At 1,500 m depth, the plume was highly enriched in Zn and Cd, and slightly enriched in Cu and P. At 3,200 m depth, the plume was highly enriched in Zn, Cd and P, and slightly enriched in Cu and Ba.

Strong positive correlations ($p < 0.001$) were observed between some elements and specific grain size fractions in the hurricane sediment plumes (Table 3). Fabian and Igor results are discussed jointly in Section 4.2.2.

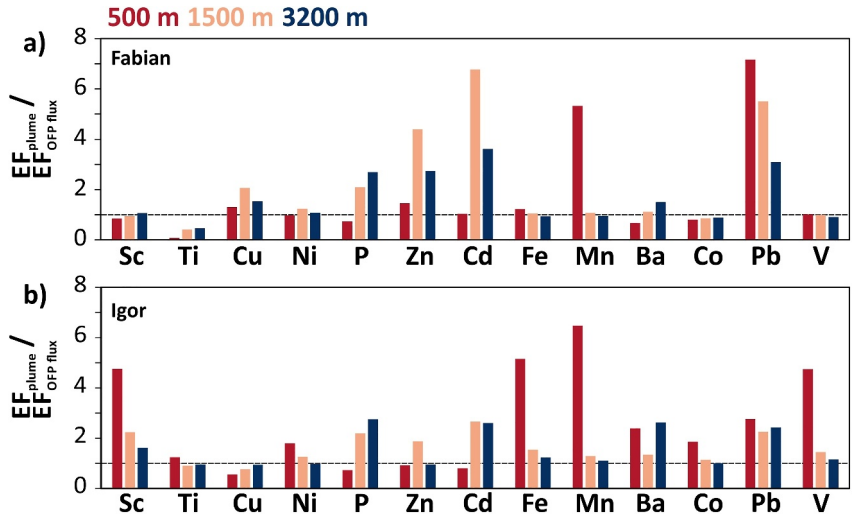

Figure 7. Ratio of elemental enrichment factors (EF) in the plume to the median EF in the oceanic flux at 500 m (red), 1,500 m (orange) and 3,200 m (blue) depths. EF ratios >1 indicate that the plume is more enriched in that element than in the typical particle flux at that depth.

4.1.3.2. Lipids

Plume lipid composition in the three trap depths had distinctive fatty acid (FA), fatty alcohol (FAL) and sterol compositions (Tables S1 and S2 in Supporting Information S1). At 500 m depth, the plume was enriched in 16:1 ω7, 18:1ω7 and 20:1ω11 monounsaturated FAs. At 1,500 m depth, the plume was enriched in long-chained saturated FA (26:0-28:0), monosaturated FAs (20:1ω11, 20:1ω9, 22:1ω11), monosaturated FALs (16:1 and

Table 3
Pearson Correlation ($p < 0.001$) of Percentage of Different Grain Particle-Size Fractions With Elemental Concentration (mg/kg) in the Fabian and Igor Sediment Plume Samples at 500, 1,500 and 3,200 m Depth

Element	Associated primarily with	%Coarse sand 500–1000 μm	% Medium sand 125–500 μm	%Fine sand 63–125 μm	% Course silt 38–63 μm	%Medium-fine silt 4–38 μm	% Clay <4 μm
Mg	Carbonates	−0.076	−0.297	−0.118	0.461	0.436	−0.764
Ca	Carbonates	0.398	−0.551	−0.607	0.575	0.728	−0.352
Sr	Carbonates	0.381	−0.462	−0.516	0.564	0.618	−0.442
Al	Lithogenic minerals	0.603	−0.172	−0.616	0.036	0.181	**0.926**
Sc	Lithogenic minerals	0.103	0.288	−0.005	−0.349	−0.334	**0.804**
Ti	Lithogenic minerals	0.384	0.335	−0.169	−0.027	−0.468	**0.889**
Fe	Lithogenic/Authigenic	0.273	0.021	−0.227	−0.272	−0.103	**0.900**
Ni	Lithogenic/Authigenic	0.669	−0.331	−0.745	0.116	0.413	**0.802**
Cu	Lithogenic	**0.777**	−0.586	−0.938	0.385	0.634	0.664
Total Si	Biogenic/Lithogenic	0.105	0.512	0.029	−0.253	−0.426	0.647
Total P	Organic matter	0.367	−0.032	−0.209	0.293	0.119	−0.349
Zn	Organic/pollutants	0.415	−0.623	−0.705	**0.773**	0.668	−0.146
Cd	Authigenic/pollutants	0.235	−0.627	−0.606	**0.906**	0.524	−0.128
Mn	Authigenic/lithogenic	0.474	−0.044	−0.503	0.076	0.026	**0.908**
Ba	Authigenic/lithogenic	0.256	0.031	−0.257	−0.039	−0.218	**0.953**
Co	Authigenic/lithogenic	0.407	−0.020	−0.429	−0.029	0.017	**0.887**
Pb	Pollutants	**0.768**	−0.547	−0.908	0.708	0.539	0.352
V	Lithogenic/Pollutants	0.314	0.009	−0.288	−0.207	−0.068	**0.909**

Note. Red and green color highlight significant negative and positive correlations, respectively. Green bold values are r > 0.7, so more significantly positively correlated.

18:1). At 3,200 m depth, the plume was enriched in saturated 14-28:0 FA, monosaturated FA (18:1ω7, 18:1ω9, 20:1ω11, 20:1ω9, 24:1), polyunsaturated FAs, saturated C_{12} and C_{16} FAL, cholesterol ($C_{27}\Delta^5$), and stanols ($C_{26}\Delta^{22}$, $C_{27}\Delta^{22}$, $C_{27}\Delta^0$, $C_{28}\Delta^0$) (See Table S2c in Supporting Information S1 for sterol abbreviation details). The 20:1ω11 FA was the only compound consistently enriched at all depths.

4.1.4. Persistence of the Advected Sediment Plume

Advected plumes primarily impacted the particle flux during the 2-week period (8 Sep-12 Oct) following Fabian passage. However, while the flux largely returned to typical values in the next sampling period, the Mg/Sr ratio of fine (<125 μm) flux material at 1,500 m depth remained elevated for two months (Figure 6), indicating continued minor presence of shallow water carbonates and their removal by suspended particle repackaging (e.g., Figure S3 in Supporting Information S1).

4.2. Hurricane Igor 2010

4.2.1. Hurricane Characteristics and Ocean Response

Hurricane Igor passed 159 km west of the OFP mooring at 2200 UTC on Sept 19, 2010, as Category 1 storm with winds of 33 m s^{-1} and a central pressure near 953 mb (Figure 2a). Igor also tracked northward at 9° but about 65% of the speed (5.7 m s^{-1}) of Fabian. Igor's eyewall passed 65 km west of Bermuda at 0200 UTC on September 20. Waves >4.6 m and a minor (0.53 m) storm surge were observed on Bermuda's south shore (Pasch & Kimberlain, 2006). No significant mesoscale features were present as Igor passed (Figure 2b).

The upper ocean temperature response to Igor was comparable to Fabian. A regional cooling of ∼3.1°C was observed in a ∼350 km-wide swath centered about 150 km to the right of the hurricane track (Figure 2a). The current meter deployed at 750 m on the OFP mooring showed an increase in currents between Sep 22 and 27 (Figure 3c). Using pressure and temperature sensors on the current meter we estimated wave isopycnal displacements (Equation 1). Estimated isopycnal displacement was 92 m using the pressure data and 89 m using the T data (assuming a T gradient of 0.026°C/m between 650 and 800 m). This displacement was comparable to that measured during Fabian. Temperature and pressure oscillations remained elevated until 27 Sep 2010.

Igor's passage also triggered massive platform-wide sediment resuspension (Figure 2c). The satellite image the day after Igor shows a sediment plume southeast of Bermuda stretching ∼60 km offshore. The similar hurricane track and plume dispersion patterns of Igor and Fabian suggest that Igor similarly generated strong deep internal waves that broke on the Pedestal, although the dynamics likely differed due to differences in hurricane characteristics (e.g., Dickey, Chang, et al., 1998).

4.2.2. Particle Export to the Deep: Bulk Fluxes and Plume Carbonate Composition

Following Hurricane Igor, TMFs increased 25-fold at 500 m, 18-fold at 1,500 m, and 6-fold at 3,200 m depths (Figure 4 and Table 1). The highest TMF was observed at 500 m depth (11.0 g m^{-2}), in contrast to Fabian where the highest TMF was observed at 1,500 m depth. The TMF at 500 m depth in the two-week period following Igor was the largest observed at the OFP site since 1978 and was equivalent to ∼70% of the annual TMF at that depth.

As in Fabian plumes, Igor plumes were overwhelmingly fine-grained (<125 μm) particles (91% at 500 m, 96% at 1,500 m and 94% at 3,200 m depths) and detrital carbonates (Table 1, Figure S2 in Supporting Information S1). The Igor sediment plume at 500 m depth had very similar grain size distribution as Fabian, with 41.5% 63–125 μm sized particles ("fine sand"), 18.0% 37–63 μm sized particles ("coarse silt"), 35.5% 4–37 μm sized particles ("medium-fine silt"), and 0.3% < 4 μm sized particles ("clay"). In contrast, the Igor plumes at 1,500 and 3,200 m depths consisted of higher percentages of 63–125 μm sized particles and lower abundances of 4–37 and 37–63 μm sized particles (Figure 5).

Carbonate percentages in the Igor plumes (97.9% at 500 m, 89.4% at 1,500 m, and 95.3% at 3,200 m) were higher than observed in the Fabian plumes. Carbonate fluxes increased by 48-fold at 500 m, 26-fold at 1,500 m, and 9-fold at 3,200 m. During the 2-week period after Igor, the carbonate flux at 500, 1,500 and 3,200 m depths accounted for ∼225%, ∼50%, and ∼25% of the annual $CaCO_3$ flux at those depths, respectively. Over the 43-day period after Igor, the carbonate fluxes at 1,500 and 3,200 m depths corresponded to ∼75% and ∼60%, respectively, of the annual carbonate flux at these depths.

As in the Fabian plume, stable isotope and elemental signatures of carbonates confirmed the Igor plume was mainly of shallow water detrital carbonate origin and most likely enriched in aragonite and high-Mg calcites. Carbonate $\delta^{13}C$ was enriched (~1.5‰), and $\delta^{18}O$ depleted (~-0.4‰). Compared with prior to Igor's passage, Mg/Ca molar ratios in the plume were 2.6-fold higher at 500 m, 2.7-fold higher at 1,500 m, and 2.3-fold higher at 3,200 m depths. Sr/Ca and Mg/Sr molar ratios also increased ~1.6-fold at all depths (Figure 6 and Figure S4 in Supporting Information S1). The larger size fractions of the Igor plume also contained large amounts of reef debris and aggregates contained abundant detrital carbonate materials (Figure S3 in Supporting Information S1).

The lithogenic and opal percentages of the Igor plumes differed from the Fabian plumes (Table 1). The lithogenic percentage of the Igor plume at 500 m (0.5%) and 1,500 m (1.8%) depths was 50% and 20% lower, respectively, than in Fabian plumes at these depths. In contrast, the opal percentage of the Igor plume at 500 m (0.9%) and 1,500 m (2.9%) depths was 50% and 5-fold higher, respectively, than in the Fabian plumes.

Despite the depth differences in the Fabian and Igor plumes, increases in POC and P fluxes were similar in both events (Table 1). POC fluxes increased 2.7-fold at 500 m, 4.1-fold at 1,500 m and 2.0-fold at 3,200 m during Igor, in comparison to 2.1-fold, 4.5-fold and 1.9-fold, respectively, during Fabian. P fluxes increased ~2.6-fold at 500 m, 3.8-fold at 1,500 m and 3.1-fold at 3,200 m during Igor, in comparison to 2.4-fold, 5.2-fold and 1.6-fold, respectively, during Fabian.

Elemental fluxes differed significantly between the Igor and Fabian events (Table 2). At 500 m depth, the relative increase in fluxes of Sc, Ti, Fe, Ba, Co and V was significantly larger during the Igor event while that of Cu and Cd was significantly lower. At 1,500 m depth, the relative increase in fluxes of Al, Ni, Fe, Ba and V and especially the pollutant elements Cu, Zn, Cd and Pd in the Igor event was significantly lower than during the Fabian event, while fluxes of Sc, Ti, Mn and Co were comparable. Smaller differences were observed at 3,200 m depth, where the plume influence on the TMF was small. The relative increase in 3,200 m fluxes of Ti, Ba and Co was slightly larger during the Igor event, while that of Cu, Zn, and Cd was slightly lower.

The lipid flux and composition also differed between the Igor and Fabian events (Tables S1 and S2 in Supporting Information S1). At 500 m depth, Total Extractable Lipid (TEL) flux was 40% lower during the Igor event while the hopanoid (HOP) flux was 50% higher, indicating a HOP enrichment in plume lipids. At 1,500 m depth, both sterol (ST) and HOP fluxes increased 3-fold but TEL flux remained constant, indicating significant enrichment in both ST and HOP in plume lipids. At 3,200 m depth, both fatty acids (FA) and ST were slightly enriched in the flux.

4.2.3. Igor Sediment Plume Composition: Non-carbonate Components

4.2.3.1. Element Enrichments and Particle Size Associations in the Fabian and Igor Plumes

Element enrichment in the Igor plume relative to the typical oceanic flux was assessed in the same manner as for the Fabian plume (Section 4.1.3.1). As with the Fabian plume, significant differences in elemental enrichments were observed in the Igor plume intercepted at the three trap depths and there were also differences in elemental composition between the Igor and Fabian plumes intercepted at the same depths (Figure 7). At 500 m depth, the Igor plume was highly enriched in Sc, Fe, Mn and V and moderately enriched in Ni, Ba, Co and Pb in comparison to the Fabian plume. The Sc, Fe and V enrichment in the Igor plume at 500 m depth was much higher than in the corresponding Fabian plume while the Pb enrichment was much lower. At 1,500 m depth, the Igor plume was moderately enriched in P, Zn, Cd and Pb, while the Fabian plume was highly enriched in Zn, Cd and Pb. At 3,200 m depth, the Igor plume was enriched in P, Cd, Ba and Pb while the Fabian plume was enriched in P, Zn, Cd and Pb.

Strong positive correlations ($p < 0.001$) were observed between elemental composition and some grain size fractions in the both the Fabian and Igor plumes (Table 3). Elements primarily associated with carbonates (Ca, Mg, and Sr) demonstrate a strong positive correlation (Pearson $r > 0.6$) with silt-sized particles (4–37 μm and 37–63 μm). This correlation is consistent with the well sorted calcareous silts in mid-slope surface sediments on the Bermuda Pedestal (Ericson et al., 1952; Lavoie et al., 1983).

In contrast, elements associated with lithogenic and authigenic minerals (Al, Sc, Ti, Fe, Ni, Cu, Mn, Ba, Co), were positively correlated (Pearson $r > 0.8$) with clay-sized particles (<4 μm). The pollutant V was also strongly positively associated with <4 μm particles, which agrees with the fact that significant amounts of vanadium are

retained in refractory organic matter or clay minerals (Breit & Wanty, 1991). In contrast, lithogenic elements Al, Ni, and Cu were strongly correlated ($r > 0.60$) with particles in the 500–1,000 μm size fraction.

Pb, Cu, Zn and Cd exhibited a strong correlation with silt-size particles (4–37 μm and 37–63 μm). Additionally Pb and Cu also were associated with the larger particle size fraction (500–1,000 μm). The association of Pb in the larger size fraction could reflect its incorporation into biogenic carbonates (Kabata-Pendias, 2001).

4.2.3.2. Lipids

The lipid composition of the Igor plume also differed among depths (Table S2 in Supporting Information S1). At 500 m, the plume was enriched in long-chain saturated FA (24-28:0), the sterols $C_{28}\Delta^{5}$ and $4\alpha C_{30}\Delta^{22}$, and the stanols $C_{27}\Delta^{0}$, and $C_{29}\Delta^{0}$. At 1,500 m, the plume was enriched saturated FA (22-28:0), monounsaturated FA (20:1ω11, 20:1ω9, 22:1ω11), saturated FAL (20-24:0), and in total sterol and stanols. At 3,200 m, the plume was enriched in saturated FA (14-16:0), monosaturated FAs, polyunsaturated FAs (20–22), saturated 16:0 FAL, the sterols $C_{27}\Delta^{5,22}$, $C_{28}\Delta^{5}$, $C_{29}\Delta^{5,22}$, $C_{29}\Delta^{5}$, $4\alpha C_{30}\Delta^{22}$, and the stanols $C_{28}\Delta^{22}$, $C_{29}\Delta^{22}$, $C_{27}\Delta^{0}$, $C_{28}\Delta^{0}$, $C_{29}\Delta^{0}$.

Although the lipid composition of the Fabian and Igor plumes was highly heterogeneous, both contained relatively high abundances of long-chain saturated FAs at 1,500 m depth and monounsaturated FAs at 1,500 and 3,200 m depths.

4.2.4. Persistence of the Igor Plume

In contrast to the Fabian event, the Igor plumes persisted in the water column much longer at the OFP site, with relatively high percentages of plume material observed in the sinking flux at 1,500 and 3,200 m for 2 months after Igor (Figure 4). Carbonate isotopic and elemental composition also evidenced the temporal persistence of plume material in the particle flux (Figure 6), with a progressive depletion in $\delta^{13}C$ (~0.3‰) and enrichment in $\delta^{18}O$ (~0.2‰) as the plume shallow-water carbonates were diluted with oceanic carbonates in the TMF. Elevated molar ratios of Mg/Ca, Sr/Ca and Mg/Sr were also observed at 1,500 and 3,200 m depths for 2 months following Igor, reflecting persistence of higher aragonite and high Mg calcite from the plumes in the TMF (Figure S4 in Supporting Information S1).

Additionally, element EFs and lipid biomarkers also evidenced the persistence of non-carbonate plume material in the TMF. The TMF at 500 m depth remained relatively enriched in Fe and V, while the TMF at 1,500 and 3,200 m depths remained relatively enriched in Sc, P, and Cd (Table S3 in Supporting Information S1). The TMF at 1,500 m depth remained elevated in saturated C_{26} and C_{28} FAs and stanols for two months, while the TMF at 3,200 m depth remained elevated in the 22:1ω11 FA and stanols (Table S4 in Supporting Information S1). Given the mesoscale current regime (e.g., Figures 2 and 3), the months long persistence of plume material in the sinking flux at the OFP site provides evidence that the plume was widely dispersed over a significant area.

5. Discussion

5.1. In Situ, Real Time Documentation of Hurricane-Generated Sediment Transport to the Deep Ocean

The two case studies presented here are the first in situ documentation of hurricane-generated sediment plumes during their transport through the water column to the deep ocean. Obtaining in situ data on sediment transport during extreme weather events is rare. Most studies have investigated sediment resuspension and dispersion using models and satellite imagery (e.g., Freeman et al., 2015; Palinkas et al., 2014; Porcile et al., 2020). However, satellite studies only reveal plume transport at near-surface depths, and lack information on advective transport deeper in the water column, which is crucial for understanding plume dispersion and deposition in offshore waters. Additionally, the studies do not provide data on plume composition, which provide information on material origins and the slope area impacted by resuspension.

This study indicates that resuspension and offshore advective transport of detrital carbonates resulting from the propagation of internal waves generated by hurricanes and their intersection with slope sediments is an underappreciated mechanism. The advection of suspended sediment plumes has been indirectly suggested by the presence of fine-grained shallow water carbonates in abyssal sediments near the Bermuda Pedestal and further offshore on the abyssal plain (Berner et al., 1976). Our data provide direct evidence of this transport and show that fine plume materials can remain in suspension in the water column for at least 2 months. Storm-advected

materials can be transported even farther offshore than documented here by regional mesoscale circulation. Thus, abyssal sediments more distant than the OFP site are likely to be influenced by advection of detrital carbonate sediments from the Bermuda carbonate Platform and Pedestal.

The resuspension and offshore advection of Bermuda Pedestal sediments to the deep waters differed significantly between Fabian and Igor. Furthermore, the distinctive composition of the plumes intercepted at different depths suggests that even during a single hurricane there can be multiple resuspension events occurring at different areas and depths on the Pedestal. The higher abundance of fine sand-sized particles (63–125 μm), and greater enrichment of Mn, Fe, and Ba in the Igor versus Fabian plume at 500 m depth suggest that the particles trapped during Igor originated from a shallower depth on the Pedestal than particles trapped during Fabian (Figures 5 and 7). Furthermore, the enrichment of pollutant elements in the Fabian versus Igor plume at 1,500 m depth suggests a resuspension area of the former where anthropogenic inputs from Bermuda accumulate, possibly a canyon on the Pedestal (Figure S1 in Supporting Information S1). This study indicates that resuspension and transport processes are likely specific to each hurricane and influenced by regional circulation. Additional characterization of grain size and geochemical fingerprints of Bermuda Platform and Pedestal sediments and the adjacent abyssal plain would further our understanding of the impact of storm-driven advection on offshore sediment transport.

These results highlight the important role that particle suspensions play in offshore transport of sediments to the deep ocean. During both hurricanes, the resuspension plumes intercepted by the sediment traps mainly consisted of fine-grained (<125 μm) detrital benthic carbonates and other fine materials that had accumulated on the Pedestal. As hydrodynamic processes resuspend and transport particles from nearshore to adjacent depositional environments, the turbulent energy of hurricane-induced internal waves generates a hydrodynamic instability that can maintain higher suspended sediment concentrations (Hosegood & Van Haren, 2004; H. van Haren et al., 2020). During transport, the coarser particles are settled out and only fine particles remain suspended (e.g., Cong et al., 2021; Dail et al., 2007; Pedrosa-Pàmies et al., 2013). Thus, fine particle suspensions can be effectively dispersed over long distances (McCave, 1984; Takesue et al., 2021).

The eventual sedimentation and removal of fine plume particles is intimately connected to biological repackaging of suspended materials into large sinking particles by zooplankton grazers within the water column. Zooplankton feeding activities throughout the water column recycle and repackage suspended materials into larger fecal pellets (e.g., Shatova et al., 2012; Urrère & Knauer, 1981; Wilson et al., 2008), leading to enhanced sedimentation of both biogenic and nonbiogenic materials (e.g., Deuser et al., 1983; Turner, 2015). The numerous large aggregates and zooplankton fecal pellets packed with fine-grained plume materials observed in the sinking flux (e.g., Figures S3c–S3d, S3g–S3h, S3k–S3i in Supporting Information S1) indicated rapid consumption and repackaging of the advected plume (Figure S3 in Supporting Information S1). Fecal pellet ballasting scales with carbonate content due to the high density of carbonate (~2.8 g cm^{-3}) (Armstrong et al., 2002), which far exceeds the typical density of pelagic zooplankton pellets (1.02–1.06 g cm^{-3}, Dilling & Alldredge, 1993). Thus, ongoing zooplankton repackaging of the fine grained plume carbonates into large rapidly sinking fecal pellets would accelerate removal of plume material from the water column by increasing its sedimentation rate.

Elemental analyses of the flux material collected between 2001 and 2015 at the OFP site (Huang & Conte, 2009; Conte et al., 2019) do not show any distinctive carbonate anomalies in the flux composition that can be attributed to shallow water carbonate advection, indicating that the hurricane-induced advection of plumes from the Bermuda Platform/Pedestal are rare occurrences. However, hurricanes have been shown to influence pelagic fluxes at the OFP site by induced nutrient upwelling and downmixing (Pedrosa-Pàmies et al., 2019). The OFP team is currently studying the impact of other major hurricanes that have passed through the OFP region.

5.2. Geochemical Impact of Hurricane-Induced Transport of Carbonate Platform Sediments to the Deep Ocean

Our observations highlight the major role that storm-induced remobilization of carbonate platform sediments play in carbonate export to the deep ocean. The massive offshore export of detrital carbonate sediments from the Pedestal by Fabian and Igor plumes resulted in the highest carbonate fluxes observed in over four decades of observations at the OFP site and accounted for approximately 80% and 60%, respectively, of the mean annual carbonate flux at the OFP site.

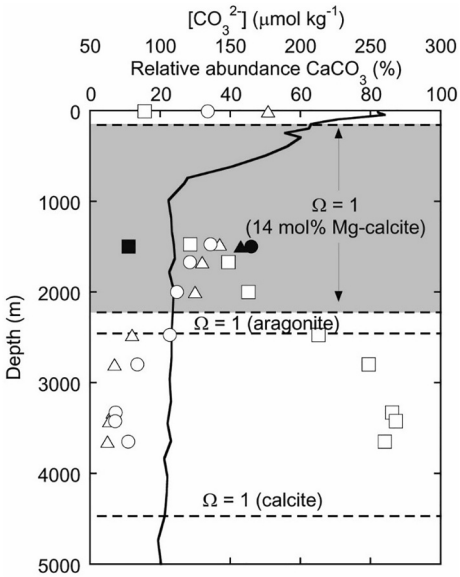

Figure 8. Seawater carbonate ion concentration close to Bermuda (black line; WOCE A20 Stn.29) and the relative carbonate mineral composition with respect to calcite (squares), aragonite (triangles) and high Mg-calcite (circles) in the sediments as a function of depth on the Bermuda pedestal (Berner et al., 1976; Chave, 1962). Solid symbols show the relative composition of the 1,500 m sediment trap carbonate material after Fabian passage. The seawater saturation horizons ($\Omega = 1$) with respect to calcite and aragonite are shown by the dashed lines. The saturation horizon with respect to 14 mol% Mg-calcite (average composition of Mg-calcite in sediment trap) is shown as a range (gray area) owing to the uncertainty associated with the solubility of this mineral phase (e.g., Morse et al., 2006).

The carbonate minerals exported by the hurricane plumes were largely of reef-sourced debris, as evidenced by the increase in Mg/Ca and Sr/Ca elemental ratios, the relative mineral composition of samples at 1,500 m following Fabian (43% aragonite: 11% calcite: 46% Mg-calcite), and the average Mg-calcite composition (14.1 mol% $MgCO_3$). The transport of reef-derived detrital carbonates from the Bermuda Pedestal to adjacent abyssal plain has been previously documented based on observations of fragments from shallow-water calcifiers such as *Halimeda* and *Homotrema rubrum* as well as detrital aragonite and high Mg-calcite in deep sea sediments (e.g., Berner et al., 1976; Lavoie & Matthews, 1983; Mackenzie et al., 1965).

The fate of reef-derived material exported to depth partly depends on the mineral solubility and the seawater saturation state. In Bermuda, the seawater saturation horizon with respect to aragonite (Ω-aragonite = 1) is found around ~2,400 m, which coincides with rapid declines of the relative proportions of aragonite and high Mg-calcite in sediments (Berner et al., 1976) (Figure 8). These trends may partly be explained by dissolution according to mineral stability as reef-sourced materials are exposed to increasing seawater undersaturation as a function of depth. The saturation horizons with respect to Mg-calcites are poorly defined, but in general, Mg-calcite with 8–12 mol% $MgCO_3$ is considered more soluble than aragonite (cf., Andersson et al., 2008; Morse et al., 2006). Hence, the reef-sourced Mg-calcites intercepted at 1,500 m depth in the Fabian plume (average composition of 14.1 mol% Mg-calcite) certainly experienced decreasing seawater saturation and potential undersaturation during resuspension and transit to depth (Figure 8).

Regardless of the precise depths of seawater undersaturation with respect to Mg-calcite minerals, the majority of $CaCO_3$ dissolution in the global ocean has been identified to occur either in the water column at depth less than 1,000 m due to metabolic or Mg-calcite dissolution, or at the seafloor following deposition in undersaturated waters (Sulpis et al., 2021). Consequently, evidence presented in this study of large resuspension and advective export of metastable aragonite and Mg-calcite minerals to the deep ocean from hurricanes passing through extensive areas of carbonate platform and slopes will most certainly contribute to increased mineral dissolution and alkalinity generation throughout the water column. In theory, this natural alkalinity enhancement could buffer part of the changes in seawater pH arising from microbial decomposition of organic material sinking toward the seafloor as well as pH changes arising from anthropogenic CO_2 uptake. It has been proposed that such buffering may promote and protect the burial of carbonates that are less soluble than the dissolving phase (e.g., Sulpis et al., 2022). Although dissolution of carbonate sediments is the ultimate sink of anthropogenic CO_2 on timescales of thousands of years (e.g., Archer et al., 1998), the potential interactions between resuspended carbonate sediments and anthropogenic CO_2 in regions impacted by tropical cyclone activity on shorter timescales (months to years) remain limited to the penetration depth of anthropogenic CO_2, which is restricted to surface and intermediate waters (<2,000 m depth) (Sabine et al., 2004). To assess the global importance of such interactions and buffering it would be necessary to estimate the total amount of carbonate exported and dissolved including the excess alkalinity generated from this process, which are not trivial tasks.

5.3. Remobilization of Non-carbonate Materials Accumulating on Carbonate Platforms

This study also documents significant offshore advection of phosphorus, lithogenic and authigenic minerals (e.g., Mn-Fe oxides, barite), pollutants, and refractory POC phases that accumulate on the Bermuda Platform and Pedestal. Substantial P enrichment in the plumes at all depths (Figure 7) evidences the strong sequestration of phosphorus through adsorption of dissolved inorganic P (i.e., phosphate) onto carbonate particle surfaces (Kitano et al., 1978). Offshore advection of P associated with shallow carbonate sediment remobilization could thus be a potentially significant nutrient source for phytoplankton in highly oligotrophic waters (e.g., Jensen et al., 1998), while plume advection at deeper depths would contribute to the P sink in abyssal sediments.

Advection of lithogenic materials was significant, particularly in the Fabian plume intercepted at 1,500 m depth (Table 1). The lithogenic material is sourced from red soils in Bermuda limestones (Lavoie & Matthews, 1983), Saharan dust deposition on the Bermuda Platform (Arimoto et al., 1992), and at deeper depths on the Bermuda Pedestal by transport of lithogenic clays that have been advected from the North American continental slope (Conte et al., 2019). Importantly, variations in lithogenic content of plumes intercepted at different depths (0.5%–4.0%) as well as differences in relative abundances of elements associated with lithogenic minerals (Sc, Ti, Fe) and sedimentary phases such as Mn-Fe oxides (Mn, Fe, Co) and barite (Ba) provide strong evidence that the plumes intercepted during Fabian and Igor originated from multiple sites and depths on the Pedestal. The significant positive relationships found among elements associated with lithogenic, authigenic, and pollutant sources indicate that these materials as well as other components that have accumulated on the Pedestal slopes can persist as suspensions in the water column for prolonged durations and thus be transported over long distances.

Of note was the significant amounts of pollutants that were remobilized and advected offshore by the hurricanes. The Fabian plume at 1,500 m depth transported the equivalent of ∼50% of the annual Pb flux at the OFP site in only 2 weeks. This Pb is sourced from both leaded gasoline used in Bermuda until the 1990s, as well as long range atmospheric transport and deposition of Pb (Church et al., 1990), and is subsequently sequestered post deposition in biogenic carbonates (Kelly et al., 2009). Interestingly, the Pb concentrations in the plumes were lower than in the typical deep particle flux (Conte et al., 2019), whose main source is advection of resuspended US continental slope sediments. This observation suggests that Pb concentrations in the North American continental margin sediments are higher than on the Bermuda Pedestal.

Zn, Cd, and Cu are widespread pollutants (Shahabi-Ghahfarokhi et al., 2021), as well as trace constituents of Mn-Fe oxides (Druce et al., 2022). The association of Zn and Pb with pollutants is evidenced by nearly identical Zn/Pb and Cd/Pb ratios (μg/μg) in the 500 m plumes advected during Fabian and Igor (Fabian: 0.41 Zn/Pb and 0.007 Cd/Pb, Igor: 0.38 Zn/Pb and 0.007 Cd/Pd) as well as comparable ratios in the 1,500 m plumes (Fabian: 0.76 Zn/Pb and 0.013 Cd/Pb, Igor: 0.61 Zn/Pb and 0.008 Cd/Pd). The differences between ratios at 500 and 1,500 m depths suggest depth variations in pollutant composition of Pedestal sediments, possibly due to temporal trends in relative emissions and subsequent downslope transport.

Finally, offshore transport of refractory POC in the plumes was evidenced by the low total lipid percentages in the POC as well as enrichment of long-chain fatty acids, which are characteristic of some reef-building corals (Latyshev et al., 1991). Although the sedimentary POC content is much lower than the oceanic flux, the massive export of Pedestal sediments resulted in a POC flux that was significantly higher than during non-hurricane conditions.

5.4. Not All Hurricanes Trigger Sediment Resuspension and Offshore Transport- Why?

Thirty-six hurricanes have passed within 300 km of Bermuda since the OFP time-series began in 1978, but resuspension plumes have only been captured at the OFP site after the passage of hurricanes Fabian and Igor (Figure S5 in Supporting Information S1). For example, even though some offshore transport of resuspended sediments was observed in satellite images during Cat. 3 Hurricane Gonzalo (Oct 2014), there was no impact on the particle flux at the OFP site despite its similar track and translational speed (7.5 m/s). This indicates that the sedimentary impacts of even quite similar hurricanes can differ substantially. One explanation is that critical determinants of a hurricane's impact depends upon the details of water column structure and mesoscale circulation which influences the downward propagation of internal waves as well as the wave interactions with the slope sediments (e.g., Dickey, Frye, et al., 1998; Firing et al., 1997; Sanford et al., 2011). For example, storm-generated near-inertial waves propagate downward more readily in an anticyclonic field (Guan et al., 2014; Jaimes & Shay, 2010; Zhai et al., 2009; Zheng et al., 2023).

Although we have no information about the specifics of the wave-slope interactions on the Pedestal nor the advective transport to the OFP site, we can conclude that the hurricane-driven deep internal waves were responsible for remobilization of sediments on the Pedestal slope. Studies on the impact of deep internal waves on sediment resuspension, transport and deposition are still scarce (Hosegood & Van Haren, 2004; Michallet & Ivey, 1999; Pomar et al., 2012 and references therein). While gravity-driven turbidity flows are a possibility (e.g., Keen & Allen, 2000; Normandeau et al., 2020), a more likely scenario is plume advection at mid water depths, which is consistent with the depth profile of the intercepted plume and their compositional differences.

It is well-documented that bathymetry and topographic conditions influence the sediment transport processes. For example, submarine canyons are well-documented to serve as efficient delivery channels for downslope transport of resuspended sediments and turbidity currents (Canals et al., 2006; Liu et al., 2012; Pedrosa-Pàmies et al., 2013; Puig et al., 2014 and references therein; Sanchez-Vidal et al., 2012; Sequeiros et al., 2019). Canyons on the Bermuda Pedestal (Figure S1 in Supporting Information S1) have been postulated to influenced the trajectory of the massive turbidite located near the Pedestal's southeast flank (Ericson et al., 1952; Lavoie & Matthews, 1983). Additionally, submarine canyons can also enhance internal-wave activity, leading to particle grain-size sorting along the canyon axis (e.g., Gardner, 1989; Hotchkiss & Wunsch, 1982). After the Fabian and Igor, it is highly plausible that part of the resuspended sediments from the upper Platform may have been funneled through the canyons on the Pedestal, enhancing the offshore dispersion.

6. Conclusions

The real-time, in situ observations described here shed light on the influence of hurricanes on sediment transport mechanisms previously inferred from geological evidence. This study highlights the complex nature of the interactions between hurricane-induced deep internal waves with bathymetry and slope characteristics leading to sediment resuspension. Furthermore, our study indicates that the impacts of individual hurricanes on sediment plume generation and advection offshore are shaped by both the specific hurricane characteristics (intensity, track and translational speed) and ocean conditions. Additionally, we show that these plumes can persist for over 2 months in the water column, underscoring their potential for widespread redistribution offshore via mesoscale circulation, and that repackaging of fine-grained plume materials into rapidly sinking particles by zooplankton grazers is a key process for its eventual sedimentation. Storm-induced remobilization and transport of shallow-water carbonates to the deep ocean has implications for the ocean carbon cycle as the export and subsequent dissolution of highly soluble aragonite and high-magnesium calcite is a source of alkalinity that could contribute to pH buffering and neutralization of anthropogenic carbon dioxide. Given recent interests in artificial interventions to enhance ocean alkalinity (e.g., NASEM, 2021), sediment transport from carbonate platforms to the deep may serve as an important natural analog that deserves further attention. Additionally, this study shows that hurricane-induced sediment resuspension can be a major process contributing to redistribution of phosphorus, lithogenic and authigenic minerals, and pollutants into deep offshore waters and eventually their abyssal sediment sink.

Our findings have implications for interpretation of sediment core hurricane reconstructions. Chemical proxies of shallow-water carbonates in abyssal sediments surrounding Bermuda could provide a valuable reconstruction of hurricane-driven advective events and a statistical constraint on past hurricane activity in the western North Atlantic.

How topographic features act in consort with hurricane characteristics to influence deep internal wave generation and the wave-slope interactions which are responsible for sediment resuspension and transport (Pomar et al., 2012) is far from clear and an important area for future research. The isolated setting of Bermuda, together with the richness of ongoing atmospheric and ocean research, makes it an exceptional model system for studying tropical cyclone-induced sediment resuspension and transport processes. This research would contribute to a better understanding of the influence of tropical cyclones on sediment transport from reef carbonate platforms throughout the tropics and subtropics and how this impacts the carbon cycle and ocean biogeochemistry.

Acknowledgments
This work and the OFP time-series is supported by the National Science Foundation Chemical Oceanography Program, most recently by Grants OCE2122619, OCE2414704, and OCE2421112. We thank Tommy Dickey for use of BTM data, Rindy Ostermann for carbonate isotopic analyses, Suilou Huang and David Koweek for elemental analyses; Emily DeFelippis, Rebecca Hopkins, and Marianna Karagiannis for lipid analyses, BATS personnel for CTD data, and Joaquim Oller for ADCP current meter data processing. We thank the R/V Atlantic Explorer crew for expert assistance on OFP mooring cruises.

Data Availability Statement

In addition to data tables published with the paper, OFP data are available from the NSF's Biological and Chemical Oceanography Data Management Office (BCO-DMO, www.bco-dmo.org/project/2286) and the corresponding author.

References

Acker, J. G., Brown, C. W., Hine, A. C., Armstrong, E., & Kuring, N. (2010). Satellite remote sensing observations and aerial photography of storm-induced neritic carbonate transport from shallow carbonate platforms. *International Journal of Remote Sensing*, *23*(14), 2853–2868. https://doi.org/10.1080/01431160110106122

Acker, J. G., Vasilkov, A., Nadeau, D., & Kuring, N. (2004). Use of SeaWiFS ocean color data to estimate neritic sediment mass transport from carbonate platforms for two hurricane-forced events. *Coral Reefs*, *23*(1), 39–47. https://doi.org/10.1007/S00338-003-0355-9/FIGURES/6

Alford, M. H., Cronin, M. F., & Klymak, J. M. (2012). Annual cycle and depth penetration of wind-generated near-inertial internal waves at ocean station papa in the Northeast Pacific. *Journal of Physical Oceanography*, *42*(6), 889–909. https://doi.org/10.1175/JPO-D-11-092.1

Alford, M. H., Mackinnon, J. A., Simmons, H. L., & Nash, J. D. (2016). Near-inertial internal gravity waves in the ocean. *Annual Review of Marine Science*, *8*(1), 95–123. https://doi.org/10.1146/Annurev-Marine-010814-015746

Anand, P., Elderfield, H., & Conte, M. H. (2003). Calibration of Mg/Ca thermometry in planktonic foraminifera from a sediment trap time series. *Paleoceanography*, *18*(2), 1050. https://doi.org/10.1029/2002PA000846

Andersson, A. J. (2014). The oceanic CaCO3 cycle. *Treatise on Geochemistry: Second Edition*, *8*, 519–542. https://doi.org/10.1016/B978-0-08-095975-7.00619-7

Andersson, A. J., Bates, N. R., & Mackenzie, F. T. (2007). Dissolution of carbonate sediments under rising pCO2 and ocean acidification: Observations from Devil's Hole, Bermuda. *Aquatic Geochemistry*, *13*(3), 237–264. https://doi.org/10.1007/S10498-007-9018-8/METRICS

Andersson, A. J., Mackenzie, F. T., & Bates, N. R. (2008). Life on the margin: Implications of ocean acidification on Mg-calcite, high latitude and cold-water marine calcifiers. *Marine Ecology Progress Series*, *373*, 265–273. https://doi.org/10.3354/meps07639

Archer, D., Kheshgi, H., & Maier-Reimer, E. (1998). Dynamics of fossil fuel CO2 neutralization by marine CaCO3. *Global Biogeochemical Cycles*, *12*(2), 259–276. https://doi.org/10.1029/98GB00744

Arimoto, R., Duce, R. A., Savoie, D. L., & Prospero, J. M. (1992). Trace elements in aerosol particles from Bermuda and Barbados: Concentrations, sources and relationships to aerosol sulfate. *Journal of Atmospheric Chemistry*, *14*(1–4), 439–457. https://doi.org/10.1007/BF00115250/METRICS

Armstrong, R. A., Lee, C., Hedges, J. I., Honjo, S., & Wakeham, S. G. (2002). A new, mechanistic model for organic carbon fluxes in the ocean based on the quantitative association of POC with ballast minerals. *Deep Sea Research Part II: Topical Studies in Oceanography*, *49*(1–3), 219–236. https://doi.org/10.1016/S0967-0645(01)00101-1

Babila, T. L., Rosenthal, Y., & Conte, M. H. (2014). Evaluation of the biogeochemical controls on B/Ca of Globigerinoides ruber white from the oceanic flux program, Bermuda. *Earth and Planetary Science Letters*, *404*, 67–76. https://doi.org/10.1016/j.epsl.2014.05.053

Berner, R. A., Berner, E. K., & Keir, R. S. (1976). Aragonite dissolution on the Bermuda pedestal: Its depth and geochemical significance. *Earth and Planetary Science Letters*, *30*(2), 169–178. https://doi.org/10.1016/0012-821X(76)90243-0

Bianucci, L., Balaguru, K., Smith, R. W., Leung, L. R., & Moriarty, J. M. (2018). Contribution of hurricane-induced sediment resuspension to coastal oxygen dynamics. *Scientific Reports*, *8*(1), 15740. https://doi.org/10.1038/s41598-018-33640-3

Bischoff, W. D. (1985). *Magnesian calcites: Physical and chemical properties and stabilities in aqueous solution of synthetic and biogenic phases*. Northwestern University ProQuest Dissertations & Theses.

Black, W. J., & Dickey, T. D. (2008). Observations and analyses of upper ocean responses to tropical storms and hurricanes in the vicinity of Bermuda. *Journal of Geophysical Research*, *113*(C08009), 1–25. https://doi.org/10.1029/2007JC004358

Boardman, M. R., & Neumann, A. C. (1984). Sources of periplatform carbonates; northwest providence channel, Bahamas. *Journal of Sedimentary Research*, *54*(4), 1110–1123. https://doi.org/10.1306/212F8571-2B24-11D7-8648000102C1865D

Breit, G. N., & Wanty, R. B. (1991). Vanadium accumulation in carbonaceous rocks: A review of geochemical controls during deposition and diagenesis. *Chemical Geology*, *91*(2), 83–97. https://doi.org/10.1016/0009-2541(91)90083-4

Browning, T. N., Sawyer, D. E., Brooks, G. R., Larson, R. A., Ramos-Scharrón, C. E., & Canals-Silander, M. (2019). Widespread deposition in a coastal bay following three major 2017 Hurricanes (Irma, Jose, and Maria). *Scientific Reports 2019*, *9*(1), 1–13. https://doi.org/10.1038/s41598-019-43062-4

Canals, M., Puig, P., de Madron, X. D., Heussner, S., Palanques, A., & Fabres, J. (2006). Flushing submarine canyons. *Nature*, *444*(7117), 354–357. https://doi.org/10.1038/nature05271

Chave, K. E. (1954). Aspects of the biogeochemistry of magnesium 1. *Calcareous Marine Organisms*, *62*(3), 266–283. https://doi.org/10.1086/626162

Chave, K. E. (1962). Factors influencing the mineralogy of carbonate sediments. *Limnology & Oceanography*, *7*(2), 218–223. https://doi.org/10.4319/lo.1962.7.2.0218

Cheriton, O. M., Storlazzi, C. D., Rosenberger, K. J., Sherman, C. E., & Schmidt, W. E. (2021). Rapid observations of ocean dynamics and stratification along a steep island coast during Hurricane María. *Science Advances*, *7*(20). https://doi.org/10.1126/SCIADV.ABF1552

Christie, W. W. (1982). *Lipid analysis: Isolation, separation, identification, and structural analysis of lipids*. Pergamon Press.

Church, T. M., Arimoto, R., Jickells, T. D., Barrie, L. A., Mart, L., Dehairs, F., et al. (1990). The long-range atmospheric transport of trace elements a critical evaluation. *The Long-Range Atmospheric Transport of Natural and Contaminant Substances. Proc., NATO Workshop, St. Georges*, *1988*, 37–58. https://doi.org/10.1007/978-94-009-0503-0_3

Coates, K. A., Fourqurean, J. W., Kenworthy, W. J., Logan, A., Manuel, S. A., & Smith, S. R. (2013). Introduction to Bermuda: Geology, Oceanography and Climate. *Coral Reefs of the World*, 115–133. https://doi.org/10.1007/978-94-007-5965-7_10

Cong, S., Wu, X., Ge, J., Bi, N., Li, Y., Lu, J., & Wang, H. (2021). Impact of Typhoon Chan-hom on sediment dynamics and morphological changes on the East China Sea inner shelf. *Marine Geology*, *440*, 106578. https://doi.org/10.1016/J.MARGEO.2021.106578

Conte, M. H., Carter, A. M., Koweek, D. A., Huang, S., & Weber, J. C. (2019). The elemental composition of the deep particle flux in the Sargasso Sea. *Chemical Geology*, *511*, 279–313. https://doi.org/10.1016/J.CHEMGEO.2018.11.001

Conte, M. H., Dickey, T. D., Weber, J. C., Johnson, R. J., & Knap, A. H. (2003). Transient physical forcing of pulsed export of bioreactive material to the deep Sargasso Sea. *Deep Sea Research Part I: Oceanographic Research Papers*, *50*(10–11), 1157–1187. https://doi.org/10.1016/S0967-0637(03)00141-9

Conte, M. H., Pedrosa-Pàmies, R., Weber, J. C., & Johnson, R. J. (2025). The climatology of the deep particle flux in the oligotrophic western North Atlantic gyre, 1978-2022. *Progress in Oceanography*, 103433. https://doi.org/10.1016/j.pocean.2025.103433

Conte, M. H., Ralph, N., & Ross, E. H. (2001). Seasonal and interannual variability in deep ocean particle fluxes at the Oceanic Flux Program (OFP)/Bermuda Atlantic Time Series (BATS) site in the western Sargasso Sea near Bermuda. *Deep Sea Research Part II: Topical Studies in Oceanography*, *48*(8–9), 1471–1505. https://doi.org/10.1016/S0967-0645(00)00150-8

Conte, M. H., & Weber, J. (2014). Particle flux in the deep Sargasso Sea: The 35-year oceanic flux program time series. *Oceanography*, *27*(1), 142–147. https://doi.org/10.5670/oceanog.2014.17

Courtney, T. A., Andersson, A. J., Bates, N. R., Collins, A., Cyronak, T., de Putron, S. J., et al. (2016). Comparing chemistry and census-based estimates of net ecosystem calcification on a rim reef in Bermuda. *Frontiers in Marine Science*, *3*(SEP), 181. https://doi.org/10.3389/FMARS.2016.00181/BIBTEX

Dail, M. B., Reide Corbett, D., & Walsh, J. P. (2007). Assessing the importance of tropical cyclones on continental margin sedimentation in the Mississippi delta region. *Continental Shelf Research*, *27*(14), 1857–1874. https://doi.org/10.1016/J.CSR.2007.03.004

Deuser, W. G. (1986). Seasonal and interannual variations in deep-water particle fluxes in the Sargasso Sea and their relation to surface hydrography. *Deep-Sea Research, Part A: Oceanographic Research Papers*, *33*(2), 225–246. https://doi.org/10.1016/0198-0149(86)90120-2

Deuser, W. G., Emeis, K., Ittekkot, V., & Degens, E. T. (1983). Fly-ash particles intercepted in the deep Sargasso Sea. *Nature*, *305*(5931), 216–218. https://doi.org/10.1038/305216a0

Deuser, W. G., Ross, E. H., & Anderson, R. F. (1981). Seasonality in the supply of sediment to the deep Sargasso Sea and implications for the rapid transfer of matter to the deep ocean. *Deep-Sea Research, Part A: Oceanographic Research Papers*, *28*(5), 495–505. https://doi.org/10.1016/0198-0149(81)90140-0

Dickey, T. D., Chang, G. C., Agrawal, Y. C., Williams, A. J., & Hill, P. S. (1998). Sediment resuspension in the wakes of Hurricanes Edouard and Hortense. *Geophysical Research Letters*, *25*(18), 3533–3536. https://doi.org/10.1029/98GL02635

Dickey, T. D., Frye, D., McNeil, J., Manov, D., Nelson, N., Sigurdson, D., et al. (1998). Upper-Ocean temperature response to Hurricane Felix as measured by the Bermuda Testbed Mooring. *Monthly Weather Review*, *126*(5), 1195–1201. https://doi.org/10.1175/1520-0493(1998)126<1195:UOTRTH>2.0.CO;2

Dickey, T. D., Zedler, S., Yu, X., Doney, S. C., Frye, D., Jannasch, H., et al. (2001). Physical and biogeochemical variability from hours to years at the Bermuda Testbed Mooring site: June 1994–March 1998. *Deep Sea Research Part II: Topical Studies in Oceanography*, *48*(8–9), 2105–2140. https://doi.org/10.1016/S0967-0645(00)00173-9

Dilling, L., & Alldredge, A. L. (1993). Can chaetognath fecal pellets contribute significantly to carbon flux? *Marine Ecology-Progress Series*, *92*, 51–58. https://doi.org/10.3354/meps092051

Druce, M., Stirling, C. H., Bostock, H. C., & Rolison, J. M. (2022). Cadmium isotope systematics in sedimentary carbonate: Extending the utility of the cadmium isotope palaeo-productivity proxy. *Geochimica et Cosmochimica Acta*, *339*, 80–96. https://doi.org/10.1016/J.GCA.2022.10.041

Dunbar, G. B., & Dickens, G. R. (2003). Late Quaternary shedding of shallow-marine carbonate along a tropical mixed siliciclastic–carbonate shelf: Great Barrier Reef, Australia. *Sedimentology*, *50*(6), 1061–1077. https://doi.org/10.1046/J.1365-3091.2003.00593.X

Ericson, D. B., Ewing, M., & Heezen, B. C. (1952). Turbidity currents and sediments in North Atlantic. *AAPG Bulletin*, *36*(3), 489–511. https://doi.org/10.1306/3D934415-16B1-11D7-8645000102C1865D

Ericson, D. B., Ewing, M., Wollin, G., & Heezen, B. C. (1961). Atlantic deep-sea sediment cores. *Geological Society of America Bulletin*, *72*(2), 193–286. https://doi.org/10.1130/0016-7606(1961)72[193:adsc]2.0.co;2

Fabricius, K. E., De'ath, G., Puotinen, M. L., Done, T., Cooper, T. F., & Burgess, S. C. (2008). Disturbance gradients on inshore and offshore coral reefs caused by a severe tropical cyclone. *Limnology & Oceanography*, *53*(2), 690–704. https://doi.org/10.4319/LO.2008.53.2.0690

Fabry, V. J., & Deuser, W. G. (1991). Aragonite and magnesian calcite fluxes to the deep Sargasso Sea. *Deep-Sea Research, Part A: Oceanographic Research Papers*, *38*(6), 713–728. https://doi.org/10.1016/0198-0149(91)90008-4

Firing, E., Lien, R.-C., & Muller, P. (1997). Observations of strong inertial oscillations after the passage of Tropical Cyclone Ofa. *Journal of Geophysical Research*, *102*(C2), 3317–3322. https://doi.org/10.1029/96JC03497

Freeman, A. M., Jose, F., Roberts, H. H., & Stone, G. W. (2015). Storm induced hydrodynamics and sediment transport in a coastal Louisiana lake. *Estuarine, Coastal and Shelf Science*, *161*, 65–75. https://doi.org/10.1016/J.ECSS.2015.04.011

Gardner, W. D. (1989). Periodic resuspension in Baltimore canyon by focusing of internal waves. *Journal of Geophysical Research*, *94*(C12), 18185–18194. https://doi.org/10.1029/JC094IC12P18185

Gray. (2019). Environmental controls on helicondoides sp. and styliola sp. In *Pteropod shell flux and isotopic composition in the sargasso sea*. University of Massachusetts Dartmouth.

Guan, S., Zhao, W., Huthnance, J., Tian, J., & Wang, J. (2014). Observed upper ocean response to typhoon Megi (2010) in the Northern South China Sea. *Journal of Geophysical Research: Oceans*, *119*(5), 3134–3157. https://doi.org/10.1002/2013JC009661

Harmelin-Vivien, M. L. (1994). The effects of storms and cyclones on coral reefs: A review. *Journal of Coastal Research*, (12), 211–231.

Heath, K. C., & Mullins, H. T. (1984). Open-ocean, off-bank transport of fine-grained carbonate sediment in the Northern Bahamas. *Geological Society Special Publication*, *15*(1), 199–208. https://doi.org/10.1144/GSL.SP.1984.015.01.13

Higgins, J. A., Blättler, C. L., Lundstrom, E. A., Santiago-Ramos, D. P., Akhtar, A. A., Crüger Ahm, A. S., et al. (2018). Mineralogy, early marine diagenesis, and the chemistry of shallow-water carbonate sediments. *Geochimica et Cosmochimica Acta*, *220*, 512–534. https://doi.org/10.1016/J.GCA.2017.09.046

Hosegood, P., & Van Haren, H. (2004). Near-bed solibores over the continental slope in the Faeroe-Shetland Channel. *Deep Sea Research Part II: Topical Studies in Oceanography*, *51*(25–26), 2943–2971. https://doi.org/10.1016/J.DSR2.2004.09.016

Hotchkiss, F. S., & Wunsch, C. (1982). Internal waves in Hudson Canyon with possible geological implications. *Deep-Sea Research, Part A: Oceanographic Research Papers*, *29*(4), 415–442. https://doi.org/10.1016/0198-0149(82)90068-1

Huang, S., & Conte, M. H. (2009). Source/process apportionment of major and trace elements in sinking particles in the Sargasso sea. *Geochimica et Cosmochimica Acta*, *73*(1), 65–90. https://doi.org/10.1016/j.gca.2008.08.023

Huang, S., Sholkovitz, E. R., & Conte, M. H. (2007). Application of high-temperature fusion for analysis of major and trace elements in marine sediment trap samples. *Limnology and Oceanography: Methods*, *5*(1), 13–22. https://doi.org/10.4319/lom.2007.5.13

Iliffe, T. M., Kvitek, R., Blasco, S., Blasco, K., & Covill, R. (2011). Search for Bermuda's deep water caves. *Hydrobiologia*, *677*(1), 157–168. https://doi.org/10.1007/s10750-011-0883-1

Jaimes, B., & Shay, L. K. (2010). Near-inertial wave wake of hurricanes Katrina and Rita over mesoscale oceanic eddies. *Journal of Physical Oceanography*, *40*(6), 1320–1337. https://doi.org/10.1175/2010JPO4309.1

James, N., Blasco, S., & Tucker, T. (2023). Holocene, mesophotic, carbonate sedimentation, Bermuda atoll margin; a submersible study. *Marine Geology*, *460*, 107049. https://doi.org/10.1016/J.MARGEO.2023.107049

Jamison-Todd, S., Stein, N., Overeem, I., Khalid, A., & Trower, E. J. (2020). Hurricane Deposits on carbonate platforms: A case study of Hurricane Irma deposits on little ambergris cay, Turks and caicos islands. *Journal of Geophysical Research: Earth Surface*, *125*(8), e2020JF005597. https://doi.org/10.1029/2020JF005597

Jasper, J. P., & Deuser, W. G. (1993). Annual cycles of mass flux and isotopic composition of pteropod shells settling into the deep Sargasso sea. *Deep-Sea Research Part I*, *40*(4), 653–669. https://doi.org/10.1016/0967-0637(93)90064-A

Jensen, H. S., McGlathery, K. J., Marino, R., & Howarth, R. W. (1998). Forms and availability of sediment phosphorus in carbonate sand of Bermuda seagrass beds. *Limnology & Oceanography*, *43*(5), 799–810. https://doi.org/10.4319/lo.1998.43.5.0799

Jones, N. S., Ridgwell, A., & Hendy, E. J. (2015). Evaluation of coral reef carbonate production models at a global scale. *Biogeosciences*, *12*(5), 1339–1356. https://doi.org/10.5194/BG-12-1339-2015

Juranek, L. W., Russell, A. D., & Spero, H. J. (2003). Seasonal oxygen and carbon isotope variability in euthecosomatous pteropods from the Sargasso Sea. *Deep-Sea Research Part I Oceanographic Research Papers*, *50*(2), 231–245. https://doi.org/10.1016/S0967-0637(02)00164-4

Kabata-Pendias, A. (2001). Trace metals in soils-a current issue in Poland. *Acta Universitatis Wratislaviensis. Prace Botaniczne*, *79*, 13–20.

Kawaguchi, Y., Nishino, S., Inoue, J., Maeno, K., Takeda, H., Oshima, K., et al. (2016). Enhanced diapycnal mixing due to near-inertial internal waves propagating through an anticyclonic eddy in the ice-free Chukchi Plateau. *Journal of Physical Oceanography*, *46*(8), 2457–2481. https://doi.org/10.1175/JPO-D-15-0150.1

Keen, T. R., & Allen, S. E. (2000). The generation of internal waves on the continental shelf by Hurricane Andrew. *Journal of Geophysical Research*, *105*(C11), 26203–26224. https://doi.org/10.1029/2000JC900137

Kelly, A. E., Reuer, M. K., Goodkin, N. F., & Boyle, E. A. (2009). Lead concentrations and isotopes in corals and water near Bermuda, 1780–2000. *Earth and Planetary Science Letters*, *283*(1–4), 93–100. https://doi.org/10.1016/J.EPSL.2009.03.045

Kitano, Y., Okumura, M., & Idogaki, M. (1978). Uptake of phosphate ions by calcium carbonate. *Geochemical Journal*, *12*(1), 29–37. https://doi.org/10.2343/GEOCHEMJ.12.29

Land, L. S., MacKenzie, F. T., & Gould, S. J. (1967). Pleistocene history of Bermuda. *Geological Society of America Bulletin*, *78*(8), 993–1006. https://doi.org/10.1130/0016-7606(1967)78[993:PHOB]2.0.CO;2

Larcombe, P., & Carter, R. M. (2004). Cyclone pumping, sediment partitioning and the development of the Great barrier reef shelf system: A review. *Quaternary Science Reviews*, *23*(1–2), 107–135. https://doi.org/10.1016/J.QUASCIREV.2003.10.003

Latyshev, N. A., Naumenko, N. V., Svetashev, V. I., & Latypov, Y. Y. (1991). Fatty acids of reef-building corals. *Marine Ecology Progress Series*, *76*, 295–301. https://doi.org/10.3354/meps076295

Laugié, M., Michel, J., Pohl, A., Poli, E., & Borgomano, J. (2019). Global distribution of modern shallow-water marine carbonate factories: A spatial model based on environmental parameters. *Scientific Reports 2019*, *9*(1), 1–14. https://doi.org/10.1038/s41598-019-52821-2

Lavoie, D., & Matthews, J. E. (1983). Sediments on the southeastern flank of the Bermuda Pedestal. *Naval Ocean Research and Development Activity Nstl Station Ms*.

Li, Y. H., & Schoonmaker, J. E. (2003). Chemical composition and mineralogy of marine sediments. *Treatise on Geochemistry*, *7*, 1–35. https://doi.org/10.1016/B0-08-043751-6/07088-2

Liu, J. T., Wang, Y.-H., Yang, R. J., Hsu, R. T., Kao, S.-J., Lin, H.-L., & Kuo, F. H. (2012). Cyclone-induced hyperpycnal turbidity currents in a submarine canyon. *Journal of Geophysical Research*, *117*(C4), 4033. https://doi.org/10.1029/2011JC007630

Lomas, M. W., Bates, N. R., Johnson, R. J., Knap, A. H., Steinberg, D. K., & Carlson, C. A. (2013). Two decades and counting: 24-years of sustained open ocean biogeochemical measurements in the Sargasso Sea. *Deep Sea Research Part II: Topical Studies in Oceanography*, *93*, 16–32. https://doi.org/10.1016/J.DSR2.2013.01.008

Mackenzie, F. T., Kulm, L. D., Cooley, R. L., & Barnhart, J. T. (1965). Homotrema rubrum (Lamarck), a sediment transport indicator. *Journal of Sedimentary Research*, *35*(1), 265–272. https://doi.org/10.1306/74D71249-2B21-11D7-8648000102C1865D

Malone, T. C., Pike, S. E., & Conley, D. J. (1993). Transient variations in phytoplankton productivity at the JGOFS Bermuda time series station. *Deep Sea Research Part I: Oceanographic Research Papers*, *40*(5), 903–924. https://doi.org/10.1016/0967-0637(93)90080-M

Markello, J. R., Koepnick, R. B., Waite, L. E., & Collins, J. F. (2008). The carbonate analogs through time (CATT) hypothesis and the global atlas of carbonate fields—A systematic and predictive look at Phanerozoic carbonate systems. In *Controls on carbonate platform and reef development*. https://doi.org/10.2110/pec.08.89.0015

Mattheus, C. R., & Yovichin, R. D. (2018). Hurricane trajectory and irregular bedrock topography as drivers of washover fan geomorphology on an isolated carbonate platform. *Journal of Coastal Research*, *34*(6), 1328–1340. https://doi.org/10.2112/JCOASTRES-D-17-00170.1

McCave, I. N. (1984). Size spectra and aggregation of suspended particles in the deep ocean. *Deep-Sea Research, Part A: Oceanographic Research Papers*, *31*(4), 329–352. https://doi.org/10.1016/0198-0149(84)90088-8

Michaels, A. F., & Knap, A. H. (1996). Overview of the U.S. JGOFS Bermuda Atlantic time-series study and the hydrostation S program. *Deep Sea Research Part II: Topical Studies in Oceanography*, *43*(2–3), 157–198. https://doi.org/10.1016/0967-0645(96)00004-5

Michallet, H., & Ivey, G. N. (1999). Experiments on mixing due to internal solitary waves breaking on uniform slopes. *Journal of Geophysical Research*, *104*(C6), 13467–13477. https://doi.org/10.1029/1999JC900037

Michel, J., Laugié, M., Pohl, A., Lanteaume, C., Masse, J. P., Donnadieu, Y., & Borgomano, J. (2019). Marine carbonate factories: A global model of carbonate platform distribution. *International Journal of Earth Sciences*, *108*(6), 1773–1792. https://doi.org/10.1007/S00531-019-01742-6/FIGURES/5

Milliman, J. D. (1993). Production and accumulation of calcium carbonate in the ocean: Budget of a nonsteady state. *Global Biogeochemical Cycles*, *7*(4), 927–957. https://doi.org/10.1029/93GB02524

Miramontes, E., Jouet, G., Thereau, E., Bruno, M., Penven, P., Guerin, C., et al. (2020). The impact of internal waves on upper continental slopes: Insights from the Mozambican margin (southwest Indian Ocean). *Earth Surface Processes and Landforms*, *45*(6), 1469–1482. https://doi.org/10.1002/esp.4818

Morse, J. W., Andersson, A. J., & Mackenzie, F. T. (2006). Initial responses of carbonate-rich shelf sediments to rising atmospheric pCO2 and "ocean acidification": Role of high Mg-calcites. *Geochimica et Cosmochimica Acta*, *70*(23), 5814–5830. https://doi.org/10.1016/J.GCA.2006.08.017

Morse, J. W., & Mackenzie, F. T. (1990). *Geochemistry of sedimentary carbonates*. Elsevier.

Mortlock, R. A., & Froelich, P. N. (1989). A simple method for the rapid determination of biogenic opal in pelagic marine sediments. *Deep-Sea Research, Part A: Oceanographic Research Papers*, *36*(9), 1415–1426. https://doi.org/10.1016/0198-0149(89)90092-7

NASEM. (2021). New report assesses the feasibility, cost, and potential impacts of Ocean-based carbon dioxide removal approaches. Retrieved from https://www.nationalacademies.org/news/2021/12/new-report-assesses-the-feasibility-cost-and-potential-impacts-of-ocean-based-carbon-dioxide-removal-approaches-recommends-u-s-research-program

Neumann, A. C. (1965). Processes of recent carbonate sedimentation in Harrington Sound, Bermuda. *Bulletin of Marine Science*, *15*(4), 987–1035.

Neumann, A. C., & Land, L. S. (1975). Lime mud deposition and calcareous algae in the Bight of Abaco, Bahamas; a budget. *Journal of Sedimentary Research*, *45*(4), 763–786. https://doi.org/10.1306/212F6E3D-2B24-11D7-8648000102C1865D

Normandeau, A., Bourgault, D., Neumeier, U., Lajeunesse, P., St-Onge, G., Gostiaux, L., & Chavanne, C. (2020). Storm-induced turbidity currents on a sediment-starved shelf: Insight from direct monitoring and repeat seabed mapping of upslope migrating bedforms. *Sedimentology*, *67*(2), 1045–1068. https://doi.org/10.1111/SED.12673

Ostermann, D. R., & Curry, W. B. (2000). Calibration of stable isotopic data: An enriched δ18O standard used for source gas mixing detection and correction. *Paleoceanography*, *15*(3), 353–360. https://doi.org/10.1029/1999PA000411

Palinkas, C. M., Halka, J. P., Li, M., Sanford, L. P., & Cheng, P. (2014). Sediment deposition from tropical storms in the upper Chesapeake Bay: Field observations and model simulations. *Continental Shelf Research*, *86*(C), 6–16. https://doi.org/10.1016/J.CSR.2013.09.012

Pasch, R. J., Blake, E. S., & Brown, D. P. (2003). *Tropical cyclone report: Hurricane Fabian, 27 August-8 September 2003*. National Hurricane Center.

Pasch, R. J., & Kimberlain, T. B. (2006). *Tropical cyclone report: Hurricane Igor, 8-21 September 2010*. National Hurricane Center.

Patrick, C. J., Kominoski, J. S., McDowell, W. H., Branoff, B., Lagomasino, D., Leon, M., et al. (2022). A general pattern of trade-offs between ecosystem resistance and resilience to tropical cyclones. *Science Advances*, *8*(9), 9155. https://doi.org/10.1126/SCIADV.ABL9155/SUPPL_FILE/SCIADV.ABL9155_CODES_S1_AND_S2.ZIP

Pedrosa-Pàmies, R., Conte, M. H., Weber, J. C., & Johnson, R. (2018). Carbon cycling in the Sargasso Sea water column: Insights from lipid biomarkers in suspended particles. *Progress in Oceanography*, *168*, 248–278. https://doi.org/10.1016/J.POCEAN.2018.08.005

Pedrosa-Pàmies, R., Conte, M. H., Weber, J. C., & Johnson, R. (2019). Hurricanes enhance labile carbon export to the deep ocean. *Geophysical Research Letters*, *46*(17–18), 10484–10494. https://doi.org/10.1029/2019GL083719

Pedrosa-Pàmies, R., Sanchez-Vidal, A., Calafat, A., Canals, M., & Durán, R. (2013). Impact of storm-induced remobilization on grain size distribution and organic carbon content in sediments from the Blanes Canyon area, NW Mediterranean Sea. *Progress in Oceanography*, *118*, 122–136. https://doi.org/10.1016/j.pocean.2013.07.023

Phillips, H. E., & Joyce, T. M. (2007). Bermuda's tale of two time series: Hydrostation S and BATS. *Journal of Physical Oceanography*, *37*(3), 554–571. https://doi.org/10.1175/JPO2997.1

Pickett, M., & Andersson, A. J. (2015). Dissolution rates of biogenic carbonates in natural seawater at different pCO2 conditions: A laboratory study. *Aquatic Geochemistry 2015*, *21*(6), 459–485. https://doi.org/10.1007/S10498-015-9261-3

Pomar, L., & Hallock, P. (2008). Carbonate factories: A conundrum in sedimentary geology. *Earth-Science Reviews*, *87*(3–4), 134–169. https://doi.org/10.1016/j.earscirev.2007.12.002

Pomar, L., Morsilli, M., Hallock, P., & Bádenas, B. (2012). Internal waves, an under-explored source of turbulence events in the sedimentary record. *Earth-Science Reviews*, *111*(1–2), 56–81. https://doi.org/10.1016/J.EARSCIREV.2011.12.005

Porcile, G., Bolla Pittaluga, M., Frascati, A., & Sequeiros, O. E. (2020). Typhoon-induced megarips as triggers of turbidity currents offshore tropical river deltas. *Communications Earth & Environment*, *1*(1), 1–13. https://doi.org/10.1038/s43247-020-0002-1

Puig, P., Palanques, A., & Martín, J. (2014). Contemporary sediment-transport processes in submarine canyons. *Annual Review of Marine Science*, *6*(1), 53–77. https://doi.org/10.1146/ANNUREV-MARINE-010213-135037

Rudnick, R. L., & Gao, S. (2003). Composition of the continental crust. *Treatise on Geochemistry*, *3*, 1–64. https://doi.org/10.1016/B0-08-043751-6/03016-4

Sabine, C. L. (1992). *Geochemistry of particulate and dissolved inorganic carbon in the central North Pacific*. University of Hawai'i at Manoa ProQuest Dissertations & Theses.

Sabine, C. L., Feely, R. A., Gruber, N., Key, R. M., Lee, K., Bullister, J. L., et al. (2004). The oceanic sink for anthropogenic CO2. *Science (New York, N.Y.)*, *305*(5682), 367–371. https://doi.org/10.1126/science.1097403

Sanchez-Vidal, A., Canals, M., Calafat, A., Lastras, G., Pedrosa-Pàmies, R., Menéndez, M., et al. (2012). Impacts on the deep-sea ecosystem by a severe coastal storm. *PLoS One*, *7*(1), e30395. https://doi.org/10.1371/journal.pone.0030395

Sanford, T. B., Price, J. F., & Girton, J. B. (2011). Upper-Ocean response to hurricane frances (2004) observed by profiling EM-APEX floats. *Journal of Physical Oceanography*, *41*(6), 1041–1056. https://doi.org/10.1175/2010JPO4313.1

Seibert, C., Feuillet, N., Ratzov, G., Beck, C., & Cattaneo, A. (2020). Seafloor morphology and sediment transfer in the mixed carbonate-siliciclastic environment of the Lesser Antilles forearc along Barbuda to St. Lucia. *Marine Geology*, *428*, 106242. https://doi.org/10.1016/J.MARGEO.2020.106242

Sequeiros, O. E., Bolla Pittaluga, M., Frascati, A., Pirmez, C., Masson, D. G., Weaver, P., et al. (2019). How typhoons trigger turbidity currents in submarine canyons. *Scientific Reports*, *9*(1), 9220. https://doi.org/10.1038/S41598-019-45615-Z

Shahabi-Ghahfarokhi, S., Josefsson, S., Apler, A., Kalbitz, K., Åström, M., & Ketzer, M. (2021). Baltic Sea sediments record anthropogenic loads of Cd, Pb, and Zn. *Environmental Science and Pollution Research International*, *28*(5), 6162–6175. https://doi.org/10.1007/S11356-020-10735-X

Shatova, O., Koweek, D., Conte, M. H., & Weber, J. C. (2012). Contribution of zooplankton fecal pellets to deep ocean particle flux in the Sargasso Sea assessed using quantitative image analysis. *Journal of Plankton Research*, *34*(10), 905–921. https://doi.org/10.1093/plankt/fbs053

Smith Warner International. (2004). Bermuda coastal erosion vulnerability assessment report. Submitted to the Government of Bermuda, Ministry of the Environment.

Spencer, L. J., DiMarco, S. F., Wang, Z., Kuehl, J. J., & Brooks, D. A. (2016). Asymmetric oceanic response to a hurricane: Deep water observations during Hurricane Isaac. *Journal of Geophysical Research: Oceans*, *121*(10), 7619–7649. https://doi.org/10.1002/2015JC011560

Spiske, M., Pilarczyk, J. E., Mitchell, S., Halley, R. B., & Otai, T. (2022). Coastal erosion and sediment reworking caused by hurricane Irma – Implications for storm impact on low-lying tropical islands. *Earth Surface Processes and Landforms*, *47*(4), 891–907. https://doi.org/10.1002/ESP.5293

Stanley, D. J., & Swift, D. J. P. (1968). Bermuda's reef-front platform: Bathymetry and significance. *Marine Geology*, *6*(6), 479–500. https://doi.org/10.1016/0025-3227(68)90028-5

Steiger. (2019). Seasonal and intra-annual variability in shell chemistry of planktonic foraminifera Globigerinoides ruber (white) morphotypes in the Sargasso Sea. *UMass Dartmouth*.

Steinberg, D. K., Carlson, C. A., Bates, N. R., Johnson, R. J., Michaels, A. F., & Knap, A. H. (2001). Overview of the US JGOFS Bermuda Atlantic time-series study (BATS): A decade-scale look at ocean biology and biogeochemistry. *Deep-Sea Research Part II Topical Studies in Oceanography*, *48*(8–9), 1405–1447. https://doi.org/10.1016/S0967-0645(00)00148-X

Stoll, H. M., Ziveri, P., Shimizu, N., Conte, M. H., & Theroux, S. (2007). Relationship between coccolith Sr/Ca ratios and coccolithophore production and export in the Arabian Sea and Sargasso Sea. *Deep-Sea Research Part II Topical Studies in Oceanography*, *54*(5–7), 581–600. https://doi.org/10.1016/j.dsr2.2007.01.003

Sulpis, O., Agrawal, P., Wolthers, M., Munhoven, G., Walker, M., & Middelburg, J. J. (2022). Aragonite dissolution protects calcite at the seafloor. *Nature Communications*, *13*(1), 1–8. https://doi.org/10.1038/s41467-022-28711-z

Sulpis, O., Jeansson, E., Dinauer, A., Lauvset, S. K., & Middelburg, J. J. (2021). Calcium carbonate dissolution patterns in the ocean. *Nature Geoscience*, *14*(6), 423–428. https://doi.org/10.1038/s41561-021-00743-y

Swart, P. K., Reijmer, J. J. G., & Otto, R. (2009). A Re-evaluation of facies on Great Bahama Bank II: Variations in the δ13C, δ18O and mineralogy of surface sediments. *Perspectives in Carbonate Geology*, 47–59. https://doi.org/10.1002/9781444312065.CH4

Takesue, R. K., Sherman, C., Ramirez, N. I., Reyes, A. O., Cheriton, O. M., Ríos, R. V., & Storlazzi, C. D. (2021). Land-based sediment sources and transport to southwest Puerto Rico coral reefs after Hurricane Maria, May 2017 to June 2018. *Estuarine, Coastal and Shelf Science*, *259*, 107476. https://doi.org/10.1016/J.ECSS.2021.107476

Teague, W. J., Jarosz, E., Wang, D. W., & Mitchell, D. a. (2007). Observed oceanic response over the upper continental slope and outer shelf during hurricane Ivan. *Journal of Physical Oceanography*, *37*(9), 2181–2206. https://doi.org/10.1175/JPO3115.1

Thran, A. C., East, M., Webster, J. M., Salles, T., & Petit, C. (2020). The influence of carbonate platforms on the geomorphological development of a mixed carbonate-siliciclastic margin (Great Barrier Reef, Australia). *Geochemistry, Geophysics, Geosystems*, *21*(4), e2020GC008915. https://doi.org/10.1029/2020GC008915

Tucker, M. E., Wright, V. P., & Dickson, J. A. D. (1990). Carbonate sedimentology.

Turner, J. T. (2015). Zooplankton fecal pellets, marine snow, phytodetritus and the ocean's biological pump. In *Progress in Oceanography*. Elsevier Ltd. https://doi.org/10.1016/j.pocean.2014.08.005

Urrère, M. A., & Knauer, G. A. (1981). Zooplankton fecal pellet fluxes and vertical transport of particulate organic material in the pelagic environment. *Journal of Plankton Research*, *3*(3), 369–387. https://doi.org/10.1093/PLANKT/3.3.369

Vacher, H. L., & Rowe, M. P. (2004). Geology and Hydrogeology of Bermuda. *Developments in Sedimentology*, *54*(C), 35–90. https://doi.org/10.1016/S0070-4571(04)80022-0

van Haren, H., Chi, W. C., Yang, C. F., Yang, Y. J., & Jan, S. (2020). Deep sea floor observations of typhoon driven enhanced ocean turbulence. *Progress in Oceanography*, *184*, 102315. https://doi.org/10.1016/J.POCEAN.2020.102315

van Haren, H., & GostIaux, L. (2012). Energy release through internal wave breaking. *Oceanography*, *25*(2), 124–131. https://doi.org/10.5670/oceanog.2012.47

Verardo, D. J., Froelich, P. N., & McIntyre, A. (1990). Determination of organic carbon and nitrogen in marine sediments using the Carlo Erba NA-1500 analyzer. *Deep-Sea Research, Part A: Oceanographic Research Papers*, *37*(1), 157–165. https://doi.org/10.1016/0198-0149(90)90034-S

Wilson, S. E., Steinberg, D. K., & Buesseler, K. O. (2008). Changes in fecal pellet characteristics with depth as indicators of zooplankton repackaging of particles in the mesopelagic zone of the subtropical and subarctic North Pacific Ocean. *Deep Sea Research Part II: Topical Studies in Oceanography*, *55*(14–15), 1636–1647. https://doi.org/10.1016/J.DSR2.2008.04.019

Zedler, S. E., Dickey, T. D., Doney, S. C., Price, J. F., Yu, X., & Mellor, G. L. (2002). Analyses and simulations of the upper ocean's response to hurricane felix at the Bermuda testbed mooring site: 13-23 August 1995. *Journal of Geophysical Research*, *107*(C12), 25–29. https://doi.org/10.1029/2001JC000969

Zhai, X., Greatbatch, R. J., Eden, C., & Hibiya, T. (2009). On the loss of wind-induced near-inertial energy to turbulent mixing in the upper ocean. *Journal of Physical Oceanography*, *39*(11), 3040–3045. https://doi.org/10.1175/2009jpo4259.1

Zheng, T., Yu, F., Ren, Q., Nan, F., Chen, Z., Liu, Y., et al. (2023). Near-inertial waves generated by typhoon MITAG under the influence of anticyclonic eddy east of Taiwan. *Frontiers in Marine Science*, *10*, 1117197. https://doi.org/10.3389/FMARS.2023.1117197/BIBTEX

Journal of Geophysical Research: Oceans

Supporting Information for

Hurricane-driven transport of Bermuda reef carbonate platform sediments to the deep ocean

R. Pedrosa-Pamies[a], M.H. Conte[a, b], J.C. Weber[a], A.J. Andersson[c]

[a] The Ecosystems Center, Marine Biological Laboratory, Woods Hole, MA, USA

[b] Bermuda Institute of Ocean Science, St. Georges GE01, Bermuda

[c] Scripps Institution of Oceanography, University of California San Diego, CA, USA

Contents of this file

Introduction

This supporting information includes one figure about the particle size change due to the hurricane passages. Also includes 4 tables, including specific lipid biomarker and elemental data.

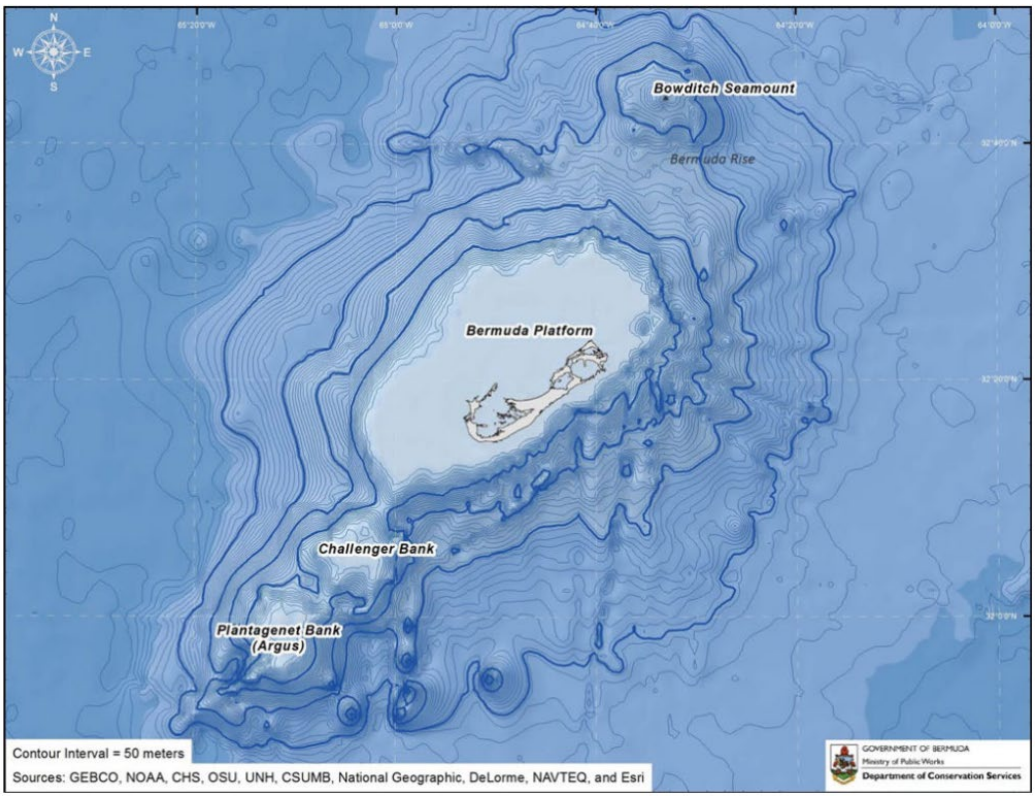

Figure S1. Bathymetry of the Bermuda Pedestal and nearby seamounts; Plantagenet and Challenger to the southwest have relatively shallow platforms, about 50 m deep, which support photosynthetic organisms; Bowditch to the northeast is a deeply submerged volcanic peak. (Figure courtesy of the Government of Bermuda, Department of Environment and Natural Resources)

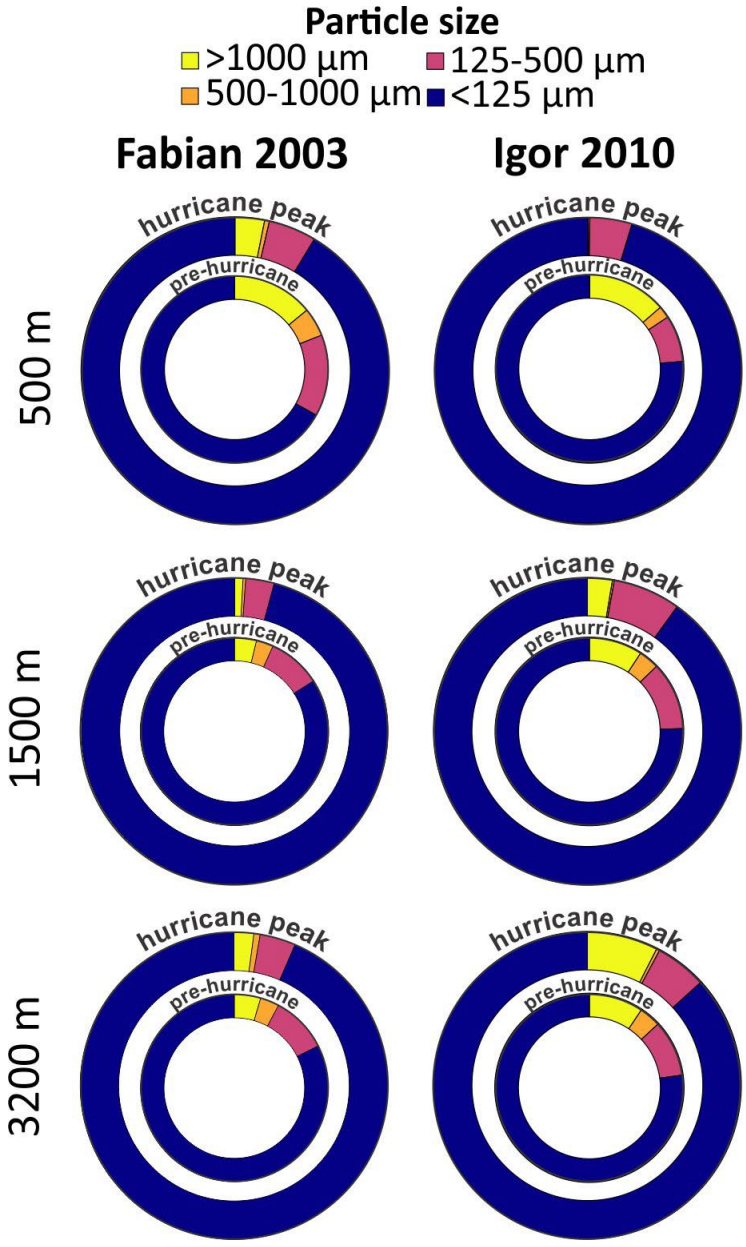

Figure S2. Particle size distributions of the flux material collected at 500, 1500 and 3200 m depths before and after hurricane passage. The ring charts show the percentage of each particle size fraction in the samples pre- and post- hurricane (inner and outer rings, respectively).

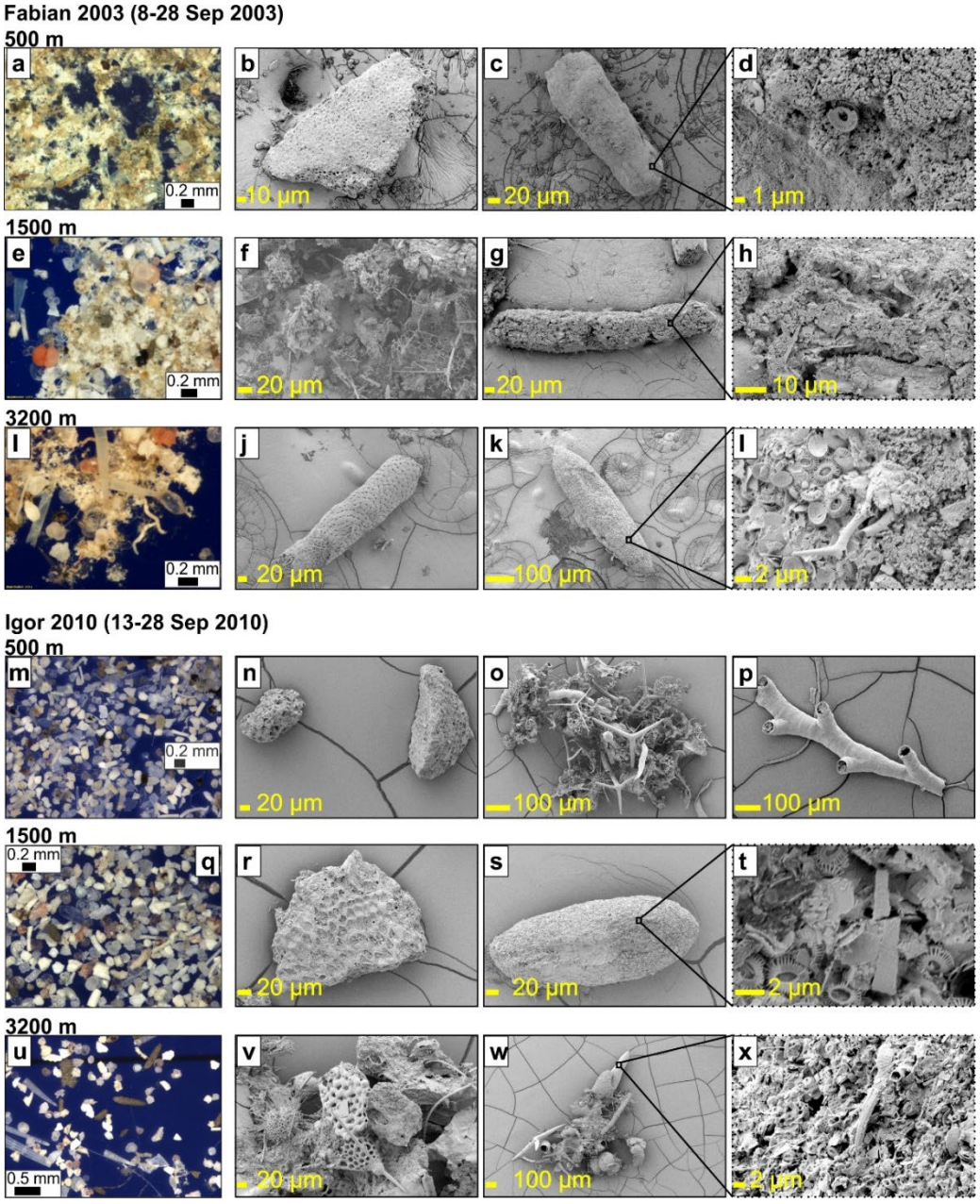

Figure S3. Microscopic images of >500 µm particles in the Fabian (a-l) and Igor (m-x) plumes. SEM images b, j, n, p, r, v, are of benthic reef particles (corals or bryozoan) and/or detrital carbonates. SEM images c, g, k, s, w, are of fecal pellets, and d, h, l, t, x are of the pellet contents. Note the abundance of fine grained detrital carbonates within the fecal pellets during the Fabian event (d, h, i).

Figure S4.

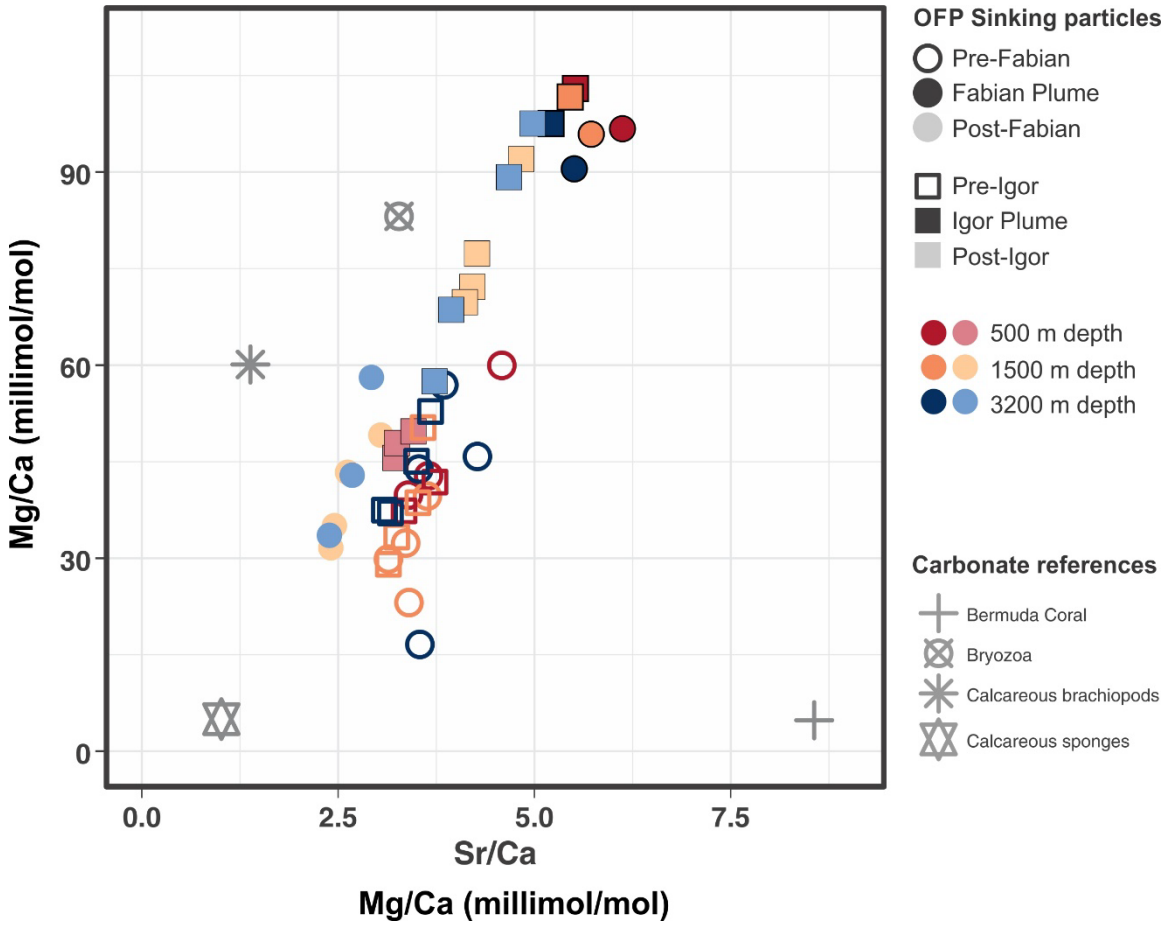

Figure S4. Mg/Ca *vs* Sr/Ca ratios (millimol/mol) from the sinking particles collected at the OFP site at 500 m (light brown), 1500 m (light blue), 3200 m (dark blue) before, during and after the passage of Fabian (preF, FABIAN, postF, respectively) and Igor (preI, IGOR, postI, respectively). Additionally, average ratios of coral collected from Hog Reef on the northern edge of the Bermuda platform (Andersson, in press), and Bryozoa, Calcareous branchiopods, and Calcareous sponges are also plotted to provide context to the values measured in the sinking particles and sediment plume (Mackenzie et al., 1983). The compositions of calcareous algae has not been included in this plot, but generally ranges from a Sr/Ca mean ratio of 2.2 to 2.9 and Mg/Ca ratios from 83 to 350 (Morse and Mackenzie, 1990). A recent study from Bermuda reported Mg/Ca ratios of 124 to 174 for coralline algae while mixed sediments had a ratio of 156 (Pickett and Andersson, 2015).

Figure S5.

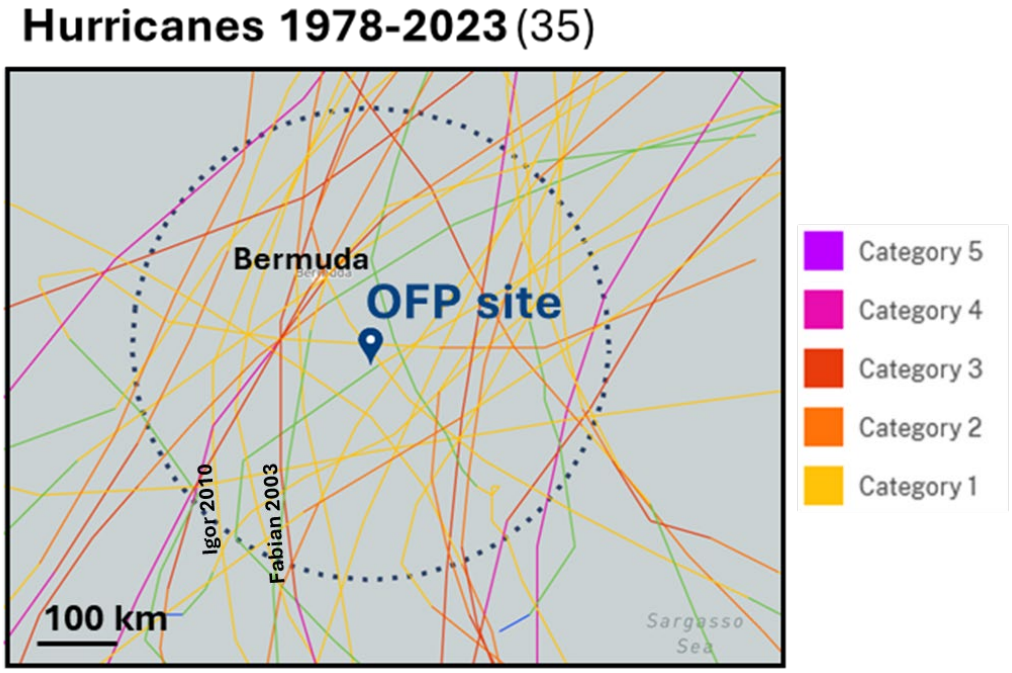

Figure S5. Hurricanes passing within 300 km (black circle) of the Bermuda from 1978 to 2023 (https://www.nhc.noaa.gov/).

	500 m			1500 m			3200 m		
	***Pre-H**	***H**	**Ratio**	***Pre-H**	***H**	**Ratio**	***Pre-H**	***H**	**Ratio**
Fabian									
TEL (µg m^{-2} d^{-1})	176.1	126.3	0.7	113.2	125.2	**1.1**	18.4	43.9	**2.4**
TEL (% of POC)	5.2	2.0	0.4	4.9	1.2	0.2	1.0	1.3	**1.3**
FA (µg m^{-2} d^{-1})	105.4	80.7	0.8	65.1	61.3	0.9	7.6	22.0	**2.9**
FAL (µg m^{-2} d^{-1})	8.7	1.8	0.2	1.6	4.6	**2.8**	0.5	0.9	**2.0**
STER (µg m^{-2} d^{-1})	27.3	17.0	0.6	20.7	17.2	0.8	2.3	7.3	**3.2**
HOP (µg m^{-2} d^{-1})	3.5	2.8	0.8	4.8	4.8	**1.0**	3.2	3.8	**1.2**
Igor									
TEL (µg m^{-2} d^{-1})	298.4	175.5	0.6	283.4	301.1	**1.1**	28.0	45.3	**1.6**
TEL (% of POC)	7.1	2.1	0.3	18.8	5.2	0.3	2.4	1.8	0.7
FA (µg m^{-2} d^{-1})	173.4	59.9	0.3	231.4	199.1	0.9	10.3	21.2	**2.1**
FAL (µg m^{-2} d^{-1})	11.7	3.7	0.3	13.5	12.1	0.9	1.9	1.9	1.0
STER (µg m^{-2} d^{-1})	59.2	52.5	0.9	8.0	25.4	**3.2**	2.8	5.8	**2.1**
HOP (µg m^{-2} d^{-1})	3.9	6.0	**1.5**	2.0	6.2	**3.1**	2.1	3.3	**1.5**

Table S1. Total extractable lipid (TEL) flux and percentage of POC, and fluxes of lipid compound classes in the sample collected before the hurricane (Pre-H) and during the hurricane plume (H). The ratio between the plume and pre-hurricane ratio (Ratio) is also given, with values of >1 difference highlighted in bold. Fatty acids (FA), Fatty alcohols (FAL), Sterols (STER) and Hopanoids (HOP).

Depth (m):	FABIAN 2003									Igor 2010								
	500			1500			3200			500			1500			3200		
	*Pre-H	*H	Ratio	*Pre-H	*H	Ratio	*Pre-H	*H	Ratio	*Pre-H	*H	Ratio	*Pre-H	*H	Ratio	*Pre-H	*H	Ratio
Saturated FA																		
14:0	3.5	2.5	0.7	1.2	1.2	1	0.0	0.1	**4.7**	4.7	3.1	0.7	8.8	10.7	***1.2***	0.4	1.1	**2.7**
16:0	29.5	17.1	0.6	23.6	13.4	0.6	1.2	4.6	**3.9**	35.5	10.4	*0.3*	87.3	53.0	0.6	2.1	4.5	***2.2***
18:0	7.1	4.5	0.6	3.3	2.8	0.8	0.5	2.7	**5**	14.3	3.4	*0.2*	8.0	15.4	***1.9***	1.3	1.3	1
20:0	0.7	0.5	0.7	0.3	0.6	***1.8***	0.1	0.4	**3**	1.5	0.7	0.5	0.8	1.7	***2***	0.2	0.2	***1.3***
22:0	0.8	0.7	0.9	0.4	0.6	***1.4***	0.2	0.5	***2.2***	2.5	0.9	*0.4*	0.7	2.8	**4.1**	0.2	0.3	***1.8***
24:0	0.9	0.7	0.8	0.4	0.6	***1.4***	0.2	0.5	***2.2***	2.1	1.1	0.5	0.6	1.5	**2.7**	0.2	0.4	***2***
26:0	0.3	0.3	1	0.3	2.6	**8.4**	0.1	0.3	***2.2***	0.2	0.6	***2.3***	0.2	0.5	**3.3**	0.2	0.0	*0.1*
28:0	0.1	0.1	0.6	0.2	2.2	**9.4**	0.1	0.1	***2.2***	0.2	0.9	**5.1**	0.0	0.3	**7.3**	0.1	0.1	***1.4***
Monounsaturated FA																		
16:1	5.0	11.5	***2.3***	3.6	3.7	1	0.7	0.8	***1.2***	27.6	8.9	*0.3*	14.5	12.2	0.8	0.4	1.5	**3.6**
18:1 ω7	2.5	10.7	**4.2**	2.9	4.0	***1.4***	0.5	1.2	**2.6**	28.5	5.7	*0.2*	10.9	8.2	0.7	0.5	1.1	***2.1***
18:1 ω9	18.4	9.2	0.5	12.7	7.7	0.6	1.2	3.0	***2.4***	14.9	3.9	*0.3*	45.8	28.6	0.6	0.9	2.8	**3**
20:1 ω11	0.2	0.4	***2.1***	0.7	1.7	***2.5***	0.0	0.2	**4.5**	0.6	0.2	*0.3*	0.5	0.9	***1.7***	0.1	0.2	**3.1**
20:1 ω9	1.4	0.5	*0.4*	0.4	1.2	**3.1**	0.2	0.6	**3**	2.1	0.4	*0.2*	3.3	7.2	***2.2***	0.1	0.7	**9**
22:1 ω11	0.7	0.3	*0.4*	0.6	1.1	***1.8***	0.1	0.1	***1.4***	1.5	0.3	*0.2*	0.5	1.3	**2.6**	0.0	0.1	**3.7**
22:1 ω9	0.9	0.3	*0.4*	0.5	1.6	**3.1**	0.3	0.4	1.1	1.5	0.3	*0.2*	1.8	2.1	1.1	0.2	0.3	***1.8***
24:1	2.0	2.7	***1.4***	0.4	3.0	**8.4**	0.1	0.4	**4**	6.2	1.4	*0.2*	2.5	1.2	0.5	0.1	0.2	**3.4**
Polyunsaturated FA																		
18:2 ω6	1.2	0.7	0.5	0.8	0.7	0.9	0.1	0.4	**3.4**	0.8	1.0	***1.3***	2.8	2.2	0.8	0.2	0.3	***2***
18:3 ω6	0.7	0.5	0.7	0.3	0.4	1.1	0.1	0.3	**5**	1.1	0.4	*0.3*	1.9	1.1	0.6	0.2	0.3	***1.3***
20:4 ω6	1.3	0.6	0.5	0.4	0.7	***1.9***	0.1	0.3	**3.1**	0.8	0.5	0.7	2.0	2.0	1	0.1	0.2	**3**
20:5 ω3	4.7	2.1	0.5	2.6	2.1	0.8	0.2	0.6	***2.5***	2.3	0.6	*0.3*	8.4	7.5	0.9	0.1	0.3	***2.3***
22:6 ω3	10.0	5.6	0.6	4.2	2.6	0.6	0.5	1.4	**2.9**	6.7	0.8	*0.1*	10.8	15.3	***1.4***	0.2	0.5	***2.4***
Odd/Branched FA																		
15:0	1.3	0.7	0.5	0.5	0.4	0.8	0.0	0.2	**4.8**	1.8	1.0	0.6	2.0	2.1	1	0.2	0.5	***2.4***
17:0	1.9	1.0	0.5	0.7	0.8	1.1	0.1	0.5	**4.3**	3.3	0.7	*0.2*	1.6	2.7	***1.6***	0.3	0.4	***1.7***
19:0	0.5	0.4	0.7	0.2	0.3	1.1	0.1	0.2	**2.7**	1.4	0.4	*0.3*	0.6	1.0	***1.7***	0.2	0.2	0.9

Table S2a. Fluxes (μg m^{-2} d^{-1}) of individual fatty acid (FA) compound in the sample collecting before the hurricane (Pre-H), and during the hurricane plume (H). The ratio between the plume and pre-hurricane ratio (Ratio) is also given, with values of >1 difference highlighted in blue. *Fabian pre-hurricane sampling period is 25 Aug-8 Sep 2003. Igor pre-hurricane sampling period is 29 Aug-12 Sep 2010, and hurricane peak period is 13-27 Sep 2010. Bold, bold/italics, and italics highlight ratios >2.5, 1.20-2.5 bold, and <0.5, respectively.

	FABIAN 2003									Igor 2010								
Depth (m):	**500**	**500**	**500**	**1500**	**1500**	**1500**	**3200**	**3200**	**3200**	**500**	**500**	**500**	**1500**	**1500**	**1500**	**3200**	**3200**	**3200**
	***Pre-H**	***H**	**Ratio**	**Pre-H**	**H**	**Ratio**	**Pre-H**	**H**	**Ratio**	**Pre-H**	**H**	**Ratio**	**Pre-H**	**H**	**Ratio**	**Pre-H**	**H**	**Ratio**
Saturated even FAL																		
16:0	3.9	0.5	*0.1*	0.9	3.1	**3.5**	0.0	0.1	**6.0**	3.6	1.0	*0.3*	3.5	2.4	0.7	0.2	0.5	**3.0**
18:0	0.8	0.4	0.5	0.1	0.1	***1.5***	0.1	0.2	***1.8***	1.6	0.7	*0.4*	1.5	1.4	0.9	0.6	0.6	1.0
20:0	0.2	0.1	0.6	0.1	0.3	***2.1***	0.1	0.1	***2.2***	0.5	0.2	*0.4*	0.2	0.4	**2.6**	0.1	0.1	0.7
22:0	0.3	0.2	0.7	0.1	0.1	***1.3***	0.1	0.1	***1.9***	0.4	0.3	0.7	0.3	0.5	***1.8***	0.1	0.1	***1.6***
24:0	0.2	0.2	0.6	0.1	0.1	***1.3***	0.1	0.1	***1.4***	0.2	0.3	***1.4***	0.1	0.4	***2.5***	0.1	0.1	***1.9***
Monounsaturated even FAL																		
18:1	1.3	0.1	*0.1*	0.0	0.1	**3.5**	0.0	0.0	***2.0***	2.6	0.3	*0.1*	2.0	0.8	*0.4*	0.1	0.1	***1.3***

Table S2b. Fluxes (μg m^{-2} d^{-1}) of individual fatty alcohol (FAL) compound in the sample collecting before the hurricane (Pre-H), and in the hurricane plume (H). The ratio between the plume and pre-hurricane ratio (Ratio) is also given, with values of >1 difference highlighted in blue. *Fabian pre-hurricane sampling period is 25 Aug-8 Sep 2003. Igor pre-hurricane sampling period is 29 Aug-12 Sep 2010, and hurricane peak period is 13-27 Sep 2010. Bold, bold/italics, and italics highlight ratios >2.5, 1.20-2.5 bold, and <0.5, respectively.

Depth (m):	FABIAN 2003									Igor 2010								
	500 *Pre-H	500 *H	500 Ratio	1500 *Pre-H	1500 *H	1500 Ratio	3200 *Pre-H	3200 *H	3200 Ratio	500 *Pre-H	500 *H	500 Ratio	1500 *Pre-H	1500 *H	1500 Ratio	3200 *Pre-H	3200 *H	3200 Ratio
Relative % to total sterols																		
$C_{27}\Delta^{5}$	17.0	7.7	0.5	7.6	6.5	0.9	0.6	4.3	**7.8**	44.4	25.4	0.6	5.1	15.2	**3.0**	1.0	1.9	***1.9***
$C_{26}\Delta^{5,22}$	0.3	0.3	0.9	0.3	0.4	***1.2***	0.1	0.1	***2.2***	0.4	0.4	1.0	0.1	0.3	***2.0***	0.1	0.1	0.9
$C_{nor27}\Delta^{5,22}$	0.9	0.7	0.8	1.3	0.9	0.7	0.1	0.2	***1.7***	1.5	1.0	0.7	0.3	0.6	***1.8***	0.2	0.3	***1.7***
$C_{27}\Delta^{5,22}$	3.0	2.6	0.9	4.7	4.2	0.9	0.3	0.5	***2***	5.4	3.8	0.7	0.7	1.7	***2.5***	0.3	0.6	***2.0***
$C_{28}\Delta^{5,22}$	0.5	0.3	0.5	0.5	0.2	*0.4*	0.1	0.2	***1.7***	0.1	0.2	***1.5***	0.1	0.4	**4.6**	0.1	0.1	***1.3***
$C_{28}\Delta^{5}$	0.3	0.4	1.1	0.5	0.8	***1.7***	0.1	0.2	***1.9***	0.4	0.8	***2.2***	0.1	0.5	**3.6**	0.1	0.2	***2.4***
$C_{29}\Delta^{5,22}$	0.6	0.5	0.9	0.5	0.6	***1.2***	0.2	0.3	***1.8***	0.6	0.9	***1.5***	0.2	0.6	**4.1**	0.1	0.2	**2.7**
$C_{29}\Delta^{5}$	0.8	0.6	0.8	1.0	0.8	0.9	0.3	0.4	***1.5***	0.9	1.0	1.1	0.3	0.9	**3.0**	0.3	0.4	***1.6***
$4\alpha C_{30}\Delta^{2}$	0.4	0.4	1.0	0.3	0.1	*0.3*	0.2	0.3	***1.9***	0.3	0.9	**2.6**	0.2	0.8	**4.8**	0.1	0.4	**2.9**
Stanols																		
$C_{26}\Delta^{22}$	0.0	0.0	0.8	0.1	0.1	1.0	0.0	0.1	**3.5**	0.1	0.2	***1.5***	0.0	0.2	**4.0**	0.0	0.0	***1.5***
$C_{27}\Delta^{22}$	0.8	0.8	1.1	0.4	0.2	0.6	0.0	0.0	**4**	0.7	0.3	0.5	0.0	0.1	**4.0**	0.1	0.1	0.8
$C_{28}\Delta^{22}$	0.2	0.1	0.5	0.5	0.4	0.8	0.1	0.0	0.8	0.7	0.7	1.0	0.1	0.4	**3.6**	0.1	0.2	***2.2***
$C_{29}\Delta^{22}$	0.3	0.3	0.9	0.7	0.4	0.5	0.1	0.1	0.8	0.4	0.6	***1.5***	0.1	0.6	**6.0**	0.1	0.3	**3.7**
$C_{27}\Delta^{0}$	1.0	1.0	1.0	0.7	0.6	0.8	0.1	0.3	***2.4***	1.7	14.0	**8.2**	0.3	1.0	**3.3**	0.1	0.3	***2.4***
$C_{28}\Delta^{0}$	0.3	0.3	1.0	0.2	0.1	*0.4*	0.0	0.1	***2.3***	0.4	0.6	***1.3***	0.1	0.3	**4.1**	0.0	0.1	**2.8**
$C_{29}\Delta^{0}$	0.2	0.2	1.0	0.4	0.3	0.8	0.1	0.1	***1.5***	0.2	0.5	***2.3***	0.1	0.4	**5.8**	0.0	0.1	**4.0**

Abbreviations: Cholest-5-en-3β-ol () ($C_{27}\Delta^{5}$, cholesterol), 24-Nor-cholesta-5,22-dien-3β-ol* ($C_{26}\Delta^{5,22}$), 27-nor-24-methylcholesta-5,22-dien-3β-ol* ($C_{nor27}\Delta^{5,22}$), Cholesta-5,22-dien-3β -ol* ($C_{27}\Delta^{5,22}$), 24-Methylcholesta-5,22-dien-3β-ol*($C_{28}\Delta^{5,22}$), 24-Methylcholesta-5,24(28)-dien-3β-ol* ($C_{28}\Delta^{5,24(28)}$), 24-Methylcholest-5-en-3β-ol* ($C_{28}\Delta^{5}$), 24-Ethylcholesta-5,22-dien-3β-ol* ($C_{29}\Delta^{5,22}$), 24-Ethylcholest-5-en-3β-ol* ($C_{29}\Delta^{5}$), 4α,23,24-Trimethyl-5a-cholest-22-en-3β-ol*($4\alpha C_{30}\Delta^{22}$). Stanols: 24-Nor-5α-cholest-22-en-3β-ol ($C_{26}\Delta^{22}$), 5α-Cholesta-22-en-3β-ol ($C_{27}\Delta^{22}$), 24-Methyl-5α-cholest-22-en-3β-ol ($C_{28}\Delta^{22}$), 24-Ehtyl-colesta-22-en-3β-ol ($C_{29}\Delta^{22}$), 5α-Cholestan-3β-ol ($C_{27}\Delta^{0}$), 24-Methyl-colestan-3β-ol ($C_{28}\Delta^{0}$), 24-Ethyl-5α-cholestan-3β-ol ($C_{29}\Delta^{0}$). (*Phytosterols)

Table S2c. Fluxes (μg m^{-2} d^{-1}) of individual sterols and stanol compounds in the sample collecting before the hurricane (Pre-H), and in the hurricane plume (H). The ratio between the plume and pre-hurricane ratio (Ratio) is also given, with values of >1 difference highlighted in blue. *Fabian pre-hurricane sampling period is 25 Aug-8 Sep 2003. Igor pre-hurricane sampling period is 29 Aug-12 Sep 2010, and hurricane peak period is 13-27 Sep 2010. Bold, bold/italics, and italics highlight ratios >2.5, 1.20-2.5 bold, and <0.5, respectively.

Depth (m)		Sampling period	Sampling duration	Sc	Ti	Cu	Ni	Total P	Zn	Cd	Fe	Mn	Ba	Co	Pb	V
500	Hurricane peak flux	13-28 Sep	15	**4.8**	***1.2***	*0.6*	***1.8***	0.7	0.9	0.8	**5.2**	**6.5**	***2.4***	***1.9***	**2.8**	**4.8**
500	Post hurricane flux	28 Sep-12 Oct	14	ND	ND	ND	ND	ND	ND	ND	ND	ND	ND	ND	ND	ND
500	Post hurricane flux	12-26 Oct	14	0.9	0.8	*0.5*	0.8	*0.5*	*0.5*	1.2	***2.1***	*0.4*	0.7	*0.2*	0.9	**2.6**
500	Post hurricane flux	26 Oct- 9 Nov	14	1.1	1.1	0.7	0.8	***1.2***	*0.6*	*0.5*	***1.9***	**3.2**	0.9	1.1	1.0	***1.8***
500	Post hurricane flux	9-23 Nov	14	1.0	1.2	0.8	1.1	*0.6*	*0.5*	0.9	***1.5***	0.9	0.8	0.7	0.9	***2.4***
1500	Hurricane peak flux	13-28 Sep	15	***2.3***	0.9	0.8	***1.3***	***2.2***	***1.9***	**2.7**	***1.6***	***1.3***	***1.3***	1.1	***2.3***	***1.5***
1500	Post hurricane flux	28 Sep-12 Oct	14	***1.7***	1.0	1.0	1.2	***1.2***	0.8	***1.7***	***1.4***	***1.4***	***1.4***	1.2	***1.6***	***1.2***
1500	Post hurricane flux	12-26 Oct	14	***1.4***	0.8	0.9	0.7	***1.5***	***2.0***	***1.3***	1.1	1.0	***1.4***	***1.2***	1.1	1.2
1500	Post hurricane flux	26 Oct- 9 Nov	14	***1.4***	0.8	1.0	0.8	***1.3***	1.1	***1.3***	1.1	1.1	1.2	1.2	1.1	***1.2***
1500	Post hurricane flux	9-23 Nov	14	***1.3***	0.8	0.9	0.7	**2.7**	**3.3**	***1.8***	1.2	1.0	1.1	1.1	1.0	1.1
3200	Hurricane peak flux	13-28 Sep	15	***1.6***	1.0	0.9	1.0	**2.8**	1.0	**2.6**	***1.2***	1.1	**2.6**	1.0	***2.4***	1.2
3200	Post hurricane flux	28 Sep-12 Oct	14	***1.6***	0.9	***1.6***	1.1	***2.4***	0.9	**6.3**	***1.3***	1.2	***1.4***	1.0	***1.5***	1.1
3200	Post hurricane flux	12-26 Oct	14	***1.4***	0.8	0.9	0.8	***1.6***	1.0	***1.3***	1.1	0.9	1.2	1.0	1.1	1.1
3200	Post hurricane flux	26 Oct- 9 Nov	14	***1.2***	0.9	1.0	0.6	***1.2***	0.8	0.7	0.9	0.9	1.2	1.1	0.8	1.0
3200	Post hurricane flux	9-23 Nov	14	***1.4***	1.1	0.7	0.8	**2.6**	0.9	***1.4***	1.1	1.0	***1.2***	1.1	1.1	1.0

Table S3. Ratio of elemental enrichment factors (EF) in the flux at 500 m, 1500 m and 3200 m depths during and after the Igor plume in comparison to the median EF in the oceanic flux. EF ratio*s* > 1 indicates that the plume is more enriched in that element than in the typical particle flux at that depth. ND- no data is available. Bold, bold/italics, and italics highlight ratios >2.5, 1.20-2.5 bold, and <0.5, respectively.

Depth (m)		Sampling period	Sampling duration	Fatty acids				Sterols						Stanols						
				24:0	26:0	´28:0	22:1w11	$C_{27}\Delta^{5}$	$C_{nor27}\Delta^{5,22}$	$C_{27}\Delta^{5,22}$	$C_{29}\Delta^{5,22}$	$C_{29}\Delta^{5}$	$4\alpha C_{30}\Delta^{2}$	$C_{26}\Delta^{22}$	$C_{27}\Delta^{22}$	$C_{28}\Delta^{22}$	$C_{29}\Delta^{22}$	$C_{27}\Delta^{0}$	$C_{28}\Delta^{0}$	$C_{29}\Delta^{0}$
500	hurricane peak flux	13-28 Sep	15	0.5	***2.4***	**5.2**	*0.2*	0.6	0.7	0.7	***1.5***	1.1	***2.5***	***1.6***	0.5	1	***1.5***	**8.2**	***1.3***	***2.3***
500	Post hurricane flux	28 Sep-12 Oct	14	*0.1*	*0.4*	*0.1*	*0*	*0*	*0.1*	*0.1*	*0.2*	*0.2*	*0.4*	*0.1*	*0.1*	*0.1*	*0.2*	*0.1*	*0.1*	*0.2*
500	Post hurricane flux	12-26 Oct	14	*0.1*	*0.3*	*0.1*	*0*	*0.2*	*0.2*	*0.2*	*0.4*	*0.3*	*0.3*	*0.3*	*0*	*0.3*	*0.3*	***1.4***	*0.2*	*0*
500	Post hurricane flux	26 Oct- 9 Nov	14	*0.3*	***1.2***	***1.2***	0.5	0.5	0.7	0.7	0.9	0.8	*0.4*	0.6	0.7	0.5	0.5	0.8	0.7	*0.2*
500	Post hurricane flux	9-23 Nov	14	*0.4*	1.1	0.9	*0.2*	0.9	1	1.1	0.9	1	0.5	0.8	0.9	0.6	0.5	1	1	0.6
1500	hurricane peak flux	13-28 Sep	15	**2.7**	**3.4**	**7.7**	**2.6**	**3**	***1.8***	***2.5***	**4.3**	**3**	**4.8**	**4.4**	**4**	**3.6**	**6.2**	**3.3**	**4.2**	**6**
1500	Post hurricane flux	28 Sep-12 Oct	14	0.6	***1.4***	***1.9***	**2.6**	*0.3*	0.5	*0.3*	0.8	0.5	0.9	0.9	**4.7**	**3**	***2.3***	1	1	*0.2*
1500	Post hurricane flux	12-26 Oct	14	1.1	***2.4***	**2.9**	0.8	***2.1***	***1.5***	***1.8***	***2.4***	***1.9***	***1.3***	***2***	**11.6**	**4.2**	***2.3***	***2.2***	***2.4***	**2.7**
1500	Post hurricane flux	26 Oct- 9 Nov	14	0.9	***2.1***	**2.6**	**7**	***1.9***	1.1	***1.6***	***2.1***	***1.6***	***1.9***	1.1	**8**	***2***	***1.8***	***2.1***	***2.5***	***1.8***
1500	Post hurricane flux	9-23 Nov	14	1.1	***1.9***	**6.8**	***2.5***	**10.1**	**3.5**	**5.5**	**3**	***2.3***	1.1	**3.2**	**19.7**	**3.3**	**2.8**	**87.8**	**9.5**	**4.5**
3200	hurricane peak flux	13-28 Sep	15	***2***	*0.1*	***1.4***	**4.1**	***1.9***	***1.6***	***2***	***2.5***	***1.6***	**3**	***1.3***	0.9	***2.3***	**3.7**	***2.3***	**2.9**	**3.6**
3200	Post hurricane flux	28 Sep-12 Oct	14	***2.4***	***2.1***	0.8	**3.8**	**6.7**	***1.9***	***2.4***	**3**	***1.8***	**3.3**	***1.8***	1.1	**3.2**	**3.6**	**3.2**	**3.6**	**4.4**
3200	Post hurricane flux	12-26 Oct	14	***1.3***	*0.1*	*0.2*	**7.5**	1	***1.2***	***1.5***	1.1	***2.1***	**3.8**	***1.2***	0.7	***2***	**7.5**	***2***	**3.4**	**4.8**
3200	Post hurricane flux	26 Oct- 9 Nov	14	1.1	1	***1.7***	***1.7***	**3**	***1.7***	***2***	**2.6**	***2***	***2.5***	1	**2.6**	***2.4***	**2.7**	**2.8**	**2.7**	**3**
3200	Post hurricane flux	9-23 Nov	14	***1.2***	***1.2***	***1.7***	**6.3**	**15.3**	***2.4***	**3.3**	**2.8**	***2***	**2.7**	1	**3.3**	***1.4***	**3.1**	**5**	**5.7**	**3.6**

Table S4. Ratios of selected lipid biomarker fluxes at 500, 1500 and 3200 m depths during and after the Igor plume in comparison to pre-hurricane fluxes. Ratios > 1 (highlighted in bold) indicates that the post-Igor flux was more enriched in that lipid compound. Bold, bold/italics, and italics highlight ratios >2.5, 1.20-2.5 bold, and <0.5, respectively. Bold, bold/italics, and italics highlight ratios >2.5, 1.20-2.5 bold, and <0.5, respectively.